frontiers in Earth Science

ORIGINAL RESEARCH
published: 26 March 2021
doi: 10.3389/feart.2021.630493

Permafrost Carbon and CO_2 Pathways Differ at Contrasting Coastal Erosion Sites in the Canadian Arctic

George Tanski[1,2,3], Lisa Bröder[2,4], Dirk Wagner[5,6], Christian Knoblauch[7,8], Hugues Lantuit[1,6], Christian Beer[7,8], Torsten Sachs[3], Michael Fritz[1], Tommaso Tesi[9], Boris P. Koch[10,11], Negar Haghipour[4,12], Timothy I. Eglinton[4], Jens Strauss[1] and Jorien E. Vonk[2]*

[1] Permafrost Research Unit, Alfred Wegener Institute Helmholtz Centre for Polar and Marine Research, Potsdam, Germany, [2] Department of Earth Sciences, Vrije Universiteit Amsterdam, Amsterdam, Netherlands, [3] GFZ German Research Centre for Geosciences, Section Remote Sensing and Geoinformatics, Potsdam, Germany, [4] Department of Earth Sciences, Swiss Federal Institute of Technology (ETH) Zürich, Zurich, Switzerland, [5] GFZ German Research Centre for Geosciences, Section Geomicrobiology, Potsdam, Germany, [6] Institute of Geosciences, Universität Potsdam, Potsdam, Germany, [7] Institute of Soil Science, Universität Hamburg, Hamburg, Germany, [8] Center for Earth System Research and Sustainability, Universität Hamburg, Hamburg, Germany, [9] Instituto di Scienze Polari – National Research Council, Bologna, Italy, [10] Biosciences Division, Alfred Wegener Institute Helmholtz Centre for Polar and Marine Research, Bremerhaven, Germany, [11] University of Applied Sciences, Bremerhaven, Germany, [12] Laboratory of Ion Beam Physics, Swiss Federal Institute of Technology (ETH) Zürich, Zurich, Switzerland

OPEN ACCESS

Edited by:
Scott Raymond Dallimore, Geological Survey of Canada, Canada

Reviewed by:
Raymond D. Ward, University of Brighton, United Kingdom
Baptiste Dafflon, Lawrence Berkeley National Laboratory, United States

***Correspondence:**
George Tanski
george.tanski@awi.de

Specialty section:
This article was submitted to Cryospheric Sciences, a section of the journal Frontiers in Earth Science

Received: 17 November 2020
Accepted: 08 March 2021
Published: 26 March 2021

Citation:
Tanski G, Bröder L, Wagner D, Knoblauch C, Lantuit H, Beer C, Sachs T, Fritz M, Tesi T, Koch BP, Haghipour N, Eglinton TI, Strauss J and Vonk JE (2021) Permafrost Carbon and CO_2 Pathways Differ at Contrasting Coastal Erosion Sites in the Canadian Arctic. Front. Earth Sci. 9:630493. doi: 10.3389/feart.2021.630493

Warming air and sea temperatures, longer open-water seasons and sea-level rise collectively promote the erosion of permafrost coasts in the Arctic, which profoundly impacts organic matter pathways. Although estimates on organic carbon (OC) fluxes from erosion exist for some parts of the Arctic, little is known about how much OC is transformed into greenhouse gases (GHGs). In this study we investigated two different coastal erosion scenarios on Qikiqtaruk – Herschel Island (Canada) and estimate the potential for GHG formation. We distinguished between a *delayed* release represented by *mud debris* draining a coastal thermoerosional feature and a *direct* release represented by *cliff debris* at a low collapsing bluff. Carbon dioxide (CO_2) production was measured during incubations at 4°C under aerobic conditions for two months and were modeled for four months and a full year. Our incubation results show that *mud debris* and *cliff debris* lost a considerable amount of OC as CO_2 (2.5 ± 0.2 and 1.6 ± 0.3% of OC, respectively). Although relative OC losses were highest in mineral *mud debris*, higher initial OC content and fresh organic matter in *cliff debris* resulted in a ∼three times higher cumulative CO_2 release (4.0 ± 0.9 compared to 1.4 ± 0.1 mg CO_2 gdw^{-1}), which was further increased by the addition of seawater. After four months, modeled OC losses were 4.9 ± 0.1 and 3.2 ± 0.3% in set-ups without seawater and 14.3 ± 0.1 and 7.3 ± 0.8% in set-ups with seawater. The results indicate that a *delayed* release may support substantial cycling of OC at relatively low CO_2 production rates during long transit times *onshore* during the Arctic warm season. By contrast, *direct* erosion may result in a single CO_2 pulse and less substantial OC

cycling *onshore* as transfer times are short. Once eroded sediments are deposited in the *nearshore*, highest OC losses can be expected. We conclude that the release of CO_2 from eroding permafrost coasts varies considerably between erosion types and residence time *onshore*. We emphasize the importance of a more comprehensive understanding of OC degradation during the coastal erosion process to improve thawed carbon trajectories and models.

Keywords: Arctic, coastal erosion, carbon cycling, biogeochemistry, greenhouse gases, carbon dioxide, biomarkers

INTRODUCTION

The Arctic is outpacing the global warming trend, which has severe impacts on ecosystems and biogeochemical pathways (Ciais et al., 2013; AMAP, 2017). With increasing temperatures, a cascade of environmental responses is initiated. Permafrost is warming and rapidly thawing, sea ice is declining in thickness and extent, seawater temperature is rising and wave and storm intensity are increasing (Manson and Solomon, 2007; Overeem et al., 2011; Schuur et al., 2015; Biskaborn et al., 2019; Dai et al., 2019). Arctic coastlines are particularly vulnerable to thaw and erosion due to the combined effects of environmental change (Barnhart et al., 2014; Fritz et al., 2017; Nielsen et al., 2020). Along with permafrost coasts, Arctic river deltas, estuaries and wetlands are increasingly impacted by sea level rise and glacier melt (Bendixen et al., 2017; Ward, 2020). These systems provide important ecosystem services (Forbes, 2019) but are currently facing changes in their sedimentation dynamics, which impacts organic matter pathways in the coastal zone (Bendixen et al., 2017; Ward, 2020). Permafrost coasts are the dominant interface between the northern landmass and the Arctic Ocean. Therefore, coastal erosion is a key driver for carbon and sediment transport into the Arctic Ocean (Stein and Macdonald, 2004; Macdonald et al., 2015; Wegner et al., 2015). Approximately two third of the Arctic coastline is composed of ice-rich and unconsolidated permafrost sediments prone to degradation, resulting in average erosion rates of 0.57 m yr^{-1} and extremes of $>$ 25 m yr^{-1} (Are et al., 2008; Jones et al., 2009, 2018; Lantuit et al., 2012; Günther et al., 2013, 2015). With erosion, the massive reservoir of seasonally unfrozen and permafrost organic carbon (OC) in the Northern Hemisphere that stores ∼1,300 Pg (10^{15} g) OC is accessed at its coastal margins (Lantuit et al., 2012; Hugelius et al., 2014; McGuire et al., 2018). Recent studies estimate that the erosion of permafrost coasts transfers up to 430 Tg yr^{-1} of sediment and 14 Tg yr^{-1} of OC into the Arctic Ocean (Wegner et al., 2015). In the current understanding of Arctic carbon cycles, coastal erosion is considered to play a modest role in the transfer of OC from land to the Arctic Ocean (McGuire et al., 2009; Stein and Macdonald, 2004; Macdonald et al., 2015). Recent studies on abrupt permafrost erosion on land, however, suggest that OC is already fundamentally altered upon permafrost thaw, erosion and transport in aquatic systems on land, during which greenhouse gases (GHGs) can be released to the atmosphere (Abbott and Jones, 2015; Mann et al., 2015; Spencer et al., 2015; Heslop et al., 2017). During these erosional processes, the composition of OC is altered substantially with a substantial fraction potentially transformed into carbon dioxide (CO_2) and methane (CH_4), depending on oxygen availability (Vonk et al., 2012; Semiletov et al., 2016; Tanski et al., 2019). Yet, the degradation of OC from thawing permafrost coastlines has barely been considered (Vonk and Gustafsson, 2013; Fritz et al., 2017).

Coastal erosion releases large amounts of readily degradable permafrost OC, which is transported on relatively short transit times from land to sea with a high potential for GHG release (Vonk et al., 2012; Tanski et al., 2019). Once it enters the ocean, OC can be either further degraded within sediments and the water column or buried in marine sediments (Vonk et al., 2014; Bröder et al., 2018; Couture et al., 2018; Grotheer et al., 2020; Jong et al., 2020). Yet, little is known about the potential GHG formation during erosion as well as within the coastal *nearshore* corridor that receives the eroded sediments before entering the marine domain. While more comprehensive information on GHG production exist for terrestrial permafrost sites and the Arctic shelf, the coast itself remains sparsely investigated with GHG measurements only available for selected locations (Vonk et al., 2012; Shakhova et al., 2010, 2015; Karlsson et al., 2015; Overduin et al., 2015; Tanski et al., 2019). Furthermore, the biogeochemical response of permafrost OC upon erosion may depend on coastal morphology and organic matter composition. Along coastlines with thermoerosional features and high bluffs, OC may encounter long transfer times *onshore* resulting in a *delayed* release to the sea with GHG formation already taking place *onshore* (**Figures 1A,B**). In contrast, at sites with low bluffs (**Figures 1C,D**), block-failure, active layer detachment slides or cliff collapse, OC may follow a more *direct* transfer pathway to the ocean. Thus, the type of erosion is strongly related to coastal morphology and may play a substantial role for the magnitude, timing and locus of GHG release. Local bathymetry and shelf morphology further determine the fate of OC and its potential for degradation offshore with rapid burial and sequestration limiting degradation but resuspension facilitating OC turnover in the *nearshore* (Solomon, 2005; Vonk et al., 2012; Hilton et al., 2015; Spencer et al., 2015; Bröder et al., 2018; Grotheer et al., 2020; Jong et al., 2020).

Although geomorphologic studies on coastal erosion processes are manifold (e.g., Barnhart et al., 2014; Günther et al., 2015; Jones et al., 2018), these studies do not target the OC fraction or relate morphology to the understanding of OC degradation and GHG dynamics. Bridging this information void on OC transformation during land-ocean-transit and the geochemical response during coastal erosion is key to better constrain biogeochemical pathways of OC in a warming

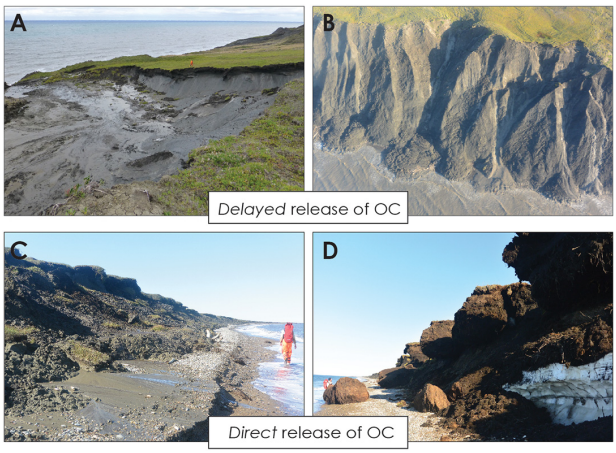

FIGURE 1 | Examples of coastal erosion types along the Yukon coast (Canadian Arctic, Beaufort Sea). Thermoerosional features and high coastal bluffs may lead to organic matter degradation *onshore* due to longer transport times and a *delayed* release into the ocean **(A,B)**. Along low bluffs, permafrost debris collapses on the beach and is removed relatively quickly by waves via a more *direct* pathway into the *nearshore* zone **(C,D)**. Photographs were taken by A. Irrgang and G. Tanski in August 2015 on Qikiqtaruk – Herschel Island **(A,B)** and the western Yukon coast **(C,D)**.

Arctic and support Earth climate modeling approaches. The objective of this study is to investigate the CO_2 production at two contrasting erosion sites along Arctic permafrost coasts to better determine the pathways and turnover of OC during transport from land to sea.

STUDY AREA

The study area Qikiqtaruk – Herschel Island is situated ∼2 km off the Yukon coast on the narrow Beaufort Sea Shelf (**Figure 2**). The local climate conditions are polar continental with mean annual air temperatures of −8.4°C (1995 to 2016) (Coch et al., 2018) and precipitation of ∼170 mm yr^{-1} (Burn, 2012). During the peak of the warm season in July temperatures are on average 7.8°C with extremes of 30°C possible (Burn, 2012). The dominant wind directions are northwest and east with storms being frequent in August and September (Dunton et al., 2006). The island is a push moraine ridge formed ∼18,000 to 23,000 years ago during the Wisconsin Glaciation with a maximum elevation of 183 m (Rampton, 1982; Pollard, 1990; Fritz et al., 2012). The sediments are composed of unconsolidated and fine-grained material of marine and glacigenic origin with glacier ice buried below the island (Blasco et al., 1990; Fritz et al., 2012). A rolling landscape incised by valleys with a lowland tundra vegetation dominated by *graminoids* and dwarf shrubs is typical for the island (Smith et al., 1989; Kennedy et al., 2001). The island is underlain with continuous permafrost with a shallow seasonal active layer of ∼40–60 cm in thickness, which has deepened by 15–25 cm since the 1980s (Kokelj et al., 2002; Burn and Zhang, 2009). The surface sediments (up to ∼1 m depth) on the island store ∼35 kg OC m^{-2} with OC storage being lower in areas of mass wasting and higher at sites of accumulation (Obu et al., 2015; Ramage et al., 2019). Permafrost sediments mainly consist of mineral soils with elevated but strongly varying OC contents when cryoturbation occurs (average 6.0 ± 4.7 wt% TOC; Tanski et al., 2017). The ground is very ice-rich with mean volumetric ground ice contents of 30–60% and maximum volumes exceeding 90%, where massive ice beds and wedge ice are present (Couture and Pollard, 2015). The open water season lasts approximately from late June to early October with landfast ice being persistent in Herschel Basin and Thetis Bay (Dunton et al., 2006). The mean tides are 0.15 m and are superimposed to a 0.66 m annual tidal cycle in late July (Huggett et al., 1975; Barnhart et al., 2014). Regional sea-level rise proceeds at rates of 1.1–3.5 mm yr^{-1} (Manson et al., 2005; James et al., 2014). The prevailing wind directions can influence water levels with northwest winds promoting a positive (higher water level) and eastern winds a negative storm surge (Hequette and Barnes, 1990; Héquette et al., 1995). The Mackenzie River plume has a strong influence on the coastal waters and transports warm water masses towards Qikiqtaruk – Herschel island, which is amplified with easterly winds (Dunton et al., 2006). Qikiqtaruk – Herschel Island is strongly impacted by thermoerosional processes and shoreline retreat. Retrogressive thaw slumps are ubiquitous and doubled in area since the 1950s (Lantuit and Pollard, 2005). On average, the island erodes at 0.68 m yr^{-1} (2000 to 2011), which is comparable to the average rates of the Yukon coast with 0.7 m yr^{-1} and the circum-Arctic with 0.57 m yr^{-1} (Lantuit et al., 2012; Obu et al., 2016; Irrgang et al., 2018). Extreme erosion rates of 14 and 22 m yr^{-1} were observed at low cliffs and active thaw slump systems, respectively (Obu et al., 2015; Cunliffe et al., 2019).

MATERIALS AND METHODS

Field Work and Sampling

Permafrost erosion debris was sampled at two active coastal erosion sites on Qikiqtaruk – Herschel Island in July and August 2017 (**Figure 2**). *Mud debris* was sampled from a mud lobe draining a retrogressive thaw slump system (**Supplementary Figure 1**) representing the *delayed* release scenario, where eroded material has relatively long residence times *onshore* before release into the ocean. We targeted a retrogressive thaw slump since these features are ubiquitous along the coastline of the western Canadian Arctic (**Figures 1A**, **2**; Pelletier and Medioli, 2014; Ramage et al., 2017). This specific thaw slump was chosen because CO_2 degradation rates of permafrost from the thaw slumps headwall are known (Tanski et al., 2019) and are used as a permafrost reference for CO_2 release *onshore*. The mud lobe draining the thaw slump is a mix of thawed permafrost, collapsed active layer and melted massive ice (e.g., buried glacier ice, wedge ice), and can be either transported directly towards the ocean or stored temporarily in mud pools on annual or decadal time scales before release into the ocean (Cray and Pollard, 2015; Tanski et al., 2017). Five samples have been taken from the mud lobe at random locations and one composite sample, *mud debris* (MUD), mixed in equal amounts from the mud lobe samples under frozen conditions in the cold lab (**Table 1**).

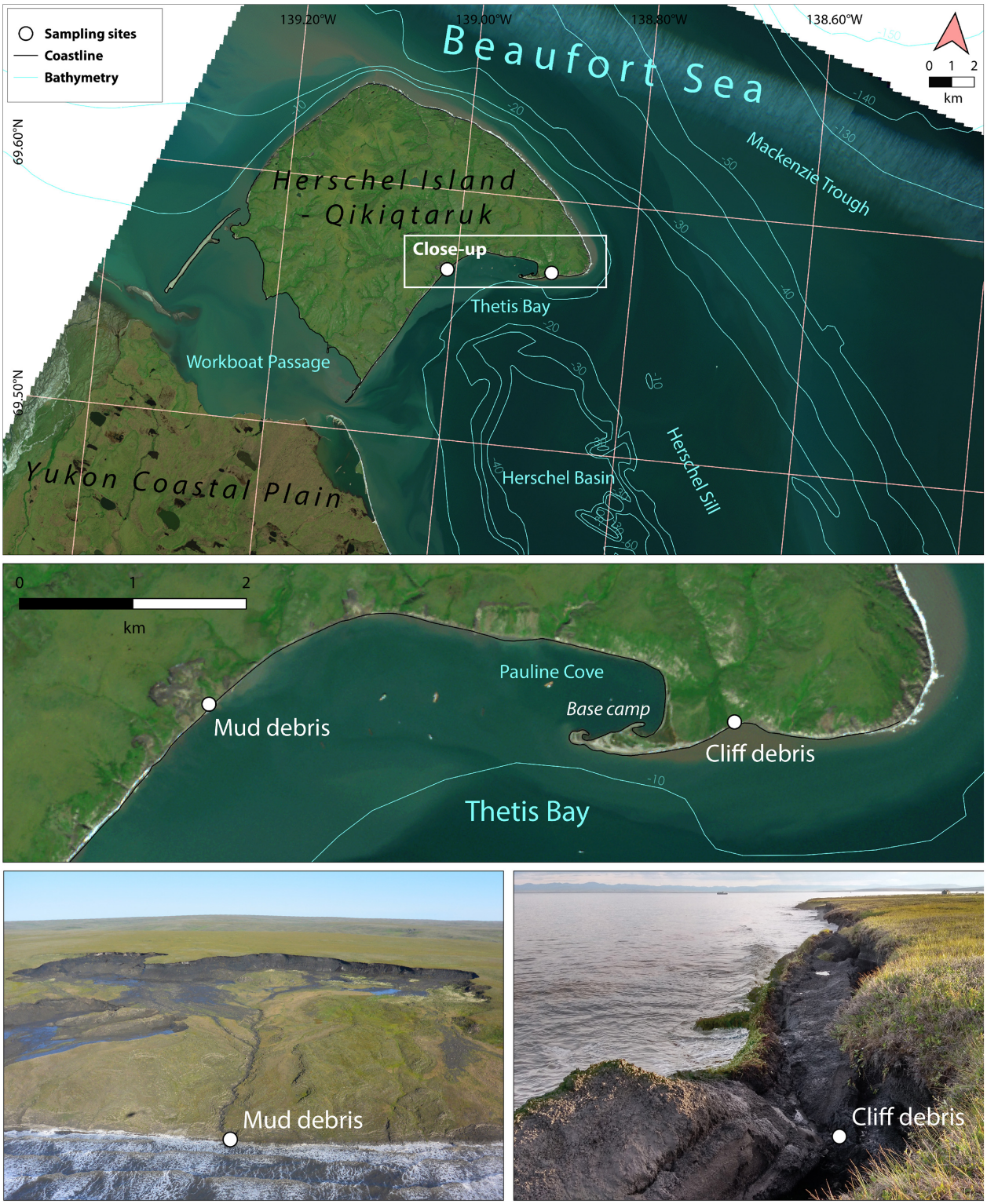

FIGURE 2 | Study area Qikiqtaruk - Herschel Island off the Yukon coast in the western Canadian Arctic. The sampling sites *mud debris* (*delayed* release) and *cliff debris* (*direct* release) are situated in the south-eastern part of the island (close-up: middle panel). The *mud debris* was taken from a mud lobe draining a retrogressive thaw slump system (lower left panel) and the *cliff debris* from an eroding cliff at the rim of an alluvial fan (lower right panel). Exact sampling locations are displayed in **Supplementary Figure 1**. Plumes and a turbid *nearshore* water column are visible and indicate substantial input and transport of eroded sediments. Satellite imagery: Sentinel 2, RGB (27 July 2017).

TABLE 1 | Summary of bulk organic matter and lipid biomarkers (*n*-alkanes) for initial (T = 0) and incubated *mud debris* (MUD) and *cliff debris* (CD) samples after two months (T = 1).

	Mud lobe	MUD (T = 0)	MUD (T = 1)	MUD* (T = 1)	Cliff	CD (T = 0)	CD (T = 1)	CD* (T = 1)
Sedimentology	n = 5	n = 1	n = 5	n = 3	n = 5	n = 1	n = 1	n = 3
Mineral SA (m^2 g^{-1})	21.5	21.5	22.2	20.7	18.0	32.4	33.6	29.2
	± 0.6	–	±1.1	± 2.9	±4.5	–	–	± 2.7
Clay (vol.%)	17.7	17.2	–	–	15.4	19.9	–	–
	± 1.5	–			± 4.5	–		
Silt (vol.%)	69.1	71.7	–	–	70.4	66.7	–	–
	± 2.1	–			± 6.9	–		
Sand (vol.%)	13.2	11.1	–	–	14.2	13.5	–	–
	± 3.3	–			± 5.4	–		
Bulk organic matter	n = 5	n = 1	n = 5	n = 5	n = 5	n = 1	n = 3	n = 3
TOC (wt%)	1.4	1.5	1.4	1.5	2.0	7.0	6.3	7.2
	± 0.03	–	±0.0	± 0.0	±0.4	–	± 0.6	±0.2
OC loading (mg m^{-2})	0.6	0.7	0.6	0.8	1.1	2.1	1.9	2.5
	± 0.02	–	±0.03	± 0.1	±0.3	–	± 0.2	±0.2
TOC/TN (atomic ratio)	10.2	10.0	9.8	11.2	11.5	14.9	13.4	14.5
	± 0.2	–	±0.3	± 0.6	±0.5	–	± 0.7	±0.9
δ^{13}C-TOC (‰)	−25.8	−25.9	−25.9	−26.1	−26.0	−26.0	−26.0	−25.9
	± 0.1	–	±0.0	± 0.5	±0.2	–	± 0.1	±0.1
Δ^{14}C-TOC (‰)	−800	−834	−836	−800	−499	−261	−253	−221
	± 75	–	±8	± 45	±100	–	± 20	±2
Age (^{14}C yr)	13,332	14,352	14,454	13,028	5679	2365	2283	1945
	± 2685	–	±418	± 1631	±1896	–	± 210	±19
***n*-alkanes**	n = 5	n = 1	n = 5	n = 4	n = 5	n = 1	n = 2	n = 3
Total[a] (μg gdw^{-1})	9.2	9.2	34.5	30.8	12.3	8.8	55.8	55.2
	± 3.4	–	±4.5	± 0.9	±5.6	–	± 6.9	±5.8
LMW[b] (μg gdw^{-1})	0.4	0.4	6.0	5.0	0.7	0.5	8.0	6.6
	± 0.2	–	±1.0	± 0.9	±0.7	–	± 2.7	±1.2
HMW[c] (μg gdw^{-1})	7.6	7.6	18.5	15.5	10.2	7.2	34.4	35.0
	± 2.9	–	±2.0	± 3.4	±4.5	–	± 4.2	±5.1
CPI[d] (C_{22-34})	4.6	4.6	2.8	2.4	6.3	5.5	3.5	4.1
	± 0.2	–	±0.3	± 0.2	±0.9	–	± 0.1	±0.5
HMW/LMW[e]	17.7	17.7	3.1	3.1	20.6	13.8	4.7	5.6
	± 5.3	–	±0.4	± 0.5	±9.3	–	± 1.1	±1.5
LMW-even/HMW-odd[f]	0.14	0.14	0.77	0.92	0.14	0.16	0.52	0.46
	± 0.04	–	±0.03	± 0.1	±0.08	–	± 0.08	±0.13

Values are given as mean with standard deviation (±) and sample size (n). The asterisk (*) indicates incubation set-ups with seawater. "Mud lobe" and "cliff" samples are in situ samples and were not incubated.

[a] $\Sigma\ C_{14-35}$.

[b] $\Sigma\ C_{14-19}$.

[c] $\Sigma\ C_{23-35}$.

[d] $CPI = 0.5\ \Sigma\ (x_i + x_{i+2} + \ldots + x_n)/\Sigma\ (x_{i-1} + x_{i+1} + \ldots + x_{n-1}) + 0.5\ \Sigma\ (x_i + x_{i+2} + \ldots + x_n)/\Sigma\ (x_{i+1} + x_{i+3} + \ldots + x_{n+1})$ with x being the concentration.

[e] $\Sigma\ C_{23-35}/\Sigma C_{14-19}$.

[f] Σ *even* C_{16-20}/Σ *odd* C_{27-31}.

The second site was a low permafrost cliff (< 5 m height) located at an alluvial fan (**Figure 2**), where *cliff debris* was collected. We chose this site to represent the *direct* release scenario with short residence time of eroded material *onshore*. This site was chosen since the erosion type is common along coasts with lower coastal bluffs (**Figures 1C,D**, **2**), where eroded material has shorter residence times *onshore* due to fast removal by wave action at high tides and storm surges (Radosavljevic et al., 2016; Cunliffe et al., 2019). We took five samples from the cliff face (Cliff, **Table 1**) and one sample from the *cliff debris* (CD) collected at the cliff toe assuming it to be an integrated signal of the *cliff* (**Table 1**). In contrast to MUD, no composite mix sample was used as we assumed that the cliff material was much more heterogeneous than the mud lobe. Thus, a mixing would have introduced an artificial bias as the mixing ratio was unclear. Surface seawater (SW) was collected approximately 2 km offshore, where water was clear and outside the range of visible erosion plumes.

All non-frozen samples from the mud debris and cliff debris (∼250–500 g wet-weight) were taken with a pre-cleaned sampling

spoon and stored in Whirl-pak bags. Samples were taken from approximately 5–10 cm below the surface, at locations where material seemed to be well-mixed during the post-erosive transport process and therefore considered representative. All (frozen) permafrost samples from the cliff face were taken with a drill hammer (Hilti, Liechtenstein) after scraping off the potentially thawed material from the cliff surface. Samples (∼500 g wet-weight) were stored in Whirl-pak bags and stored frozen in a cooler immediately to avoid thaw. Seawater was taken from the sea surface in pre-rinsed (three times) 1L Nalgene bottles. All sampled materials, including seawater, were kept frozen at −20°C until further processing in the laboratories.

Incubation Set-Ups

We simulated the erosion of *mud debris* and *cliff debris onshore* as well as in the *nearshore* in a laboratory incubation experiment at GFZ Potsdam to assess potential carbon pathways in this coastal transition zone. *Onshore* refers to incubation set-ups without seawater, mimicking erosion on land, while *nearshore* set-ups with seawater added were designed to mimic erosion into the seawater column. Frozen *mud debris* and *cliff debris* samples were homogenized and subsamples of ∼20 g placed into 120 ml glass vials (autoclaved at 125°C) at −15°C in a cold lab. The frozen seawater (SW) sample was melted slowly at 7°C in a cool (dark) room and shaken thoroughly. Just before the start of the incubation ∼30 ml of unfiltered seawater was added to the glass vials with subsamples for the *nearshore* incubation set-ups. Afterwards, the vials were sealed with a rubber septum and the headspace (ca. 90 to 100 ml) was flushed with synthetic air (Linde, Germany) consisting of 20% oxygen (O_2) and 80% nitrogen (N_2). Vials were then placed in an incubator at 4°C shielded from light. Aerobic conditions were applied by flushing the headspace with synthetic air after each CO_2 measurement to represent venting and associated oxygen supply likely occurring during the erosion process *onshore* as well as in the immediate *nearshore*. The incubation period was set to two months to capture the initial period of highest CO_2 production (Tanski et al., 2019) and conducted at 4°C as it is close to the ambient Arctic sea surface temperatures and comparable to most published permafrost incubation studies (Dutta et al., 2006; Lee et al., 2012; Schädel et al., 2014).

Hydrochemistry

Basic hydrochemical parameters pH and electrical conductivity were measured with a 3430 Digital Multiparameter meter (WTW, Germany) at room temperature at AWI Potsdam, Germany. Seawater was filtered with a 0.7 μm GF/F filter (Whatman, United Kingdom) and acidified with HCl (suprapur grade 30%) to pH 2. Dissolved organic carbon (DOC) and dissolved nitrogen (DN) concentrations were analyzed with a Shimadzu analyzer (Shimadzu, Japan) at AWI Bremerhaven, Germany.

Gas Measurements and Mass Calculation

CO_2 and CH_4 concentrations were measured with a 7890A GC (Agilent, United States) at GFZ Potsdam, Germany. Gas samples were taken on a regular basis (every other day during the first two weeks and two times a week afterwards) with a gastight syringe from the headspace of the vials and were immediately injected into the gas chromatograph. Afterwards, the headspace was flushed with synthetic air to reset aerobic conditions. After each measurement, glass vials were shaken to simulate mixing of sediments during mass movement *onshore* and by wave action and currents in the *nearshore*. The gas production was measured in parts per million (ppm) and normalized to gram dry weight (gdw^{-1}) of initial sediment. The total amount of CO_2 and CH_4 (μmol) was calculated following the methodology by Knoblauch et al. (2018) using gas concentration, headspace volume, water volume, pH, temperature and solubility including carbonate and bicarbonate concentrations for CO_2 calculations (Millero et al., 2007). All gas that remained in the glass vials after flushing was accounted for by assuming that CO_2 in the headspace was completely removed with flushing but dissolved inorganic carbon (DIC) remained in the glass vials. The derived amount of CO_2 in μmol was normalized to gdw^{-1} and recalculated into mg CO_2 gdw^{-1} using the molar mass (M) of CO_2 (44). In this study, we only report CO_2 as incubations conditions were aerobic.

Bulk Elemental and Isotopic Analyses

Sediments were weighed, freeze-dried and homogenized before chemical analysis. Elemental and stable carbon isotope analysis was conducted at AWI Potsdam, Germany, following established methodology (e.g., Schirrmeister et al., 2018). Total carbon (TC) and total nitrogen (TN) contents were measured with a VARIO EL III element analyzer (Elementar, Germany) and total organic carbon (TOC) with a VARIO MAX C analyzer (Elementar, Germany), both with a device-specific accuracy of ± 0.1wt %. For stable carbon isotope (δ^{13}C-TOC), carbonates were removed from sediments with 1.3 molar hydrochloric acid (HCl) at 95°C for three hours. Stable carbon isotopes were then measured at the Isotope Facility at AWI Potsdam with a Delta-V-Advantage mass spectrometer (MS) (Thermo Fisher Scientific, Germany) coupled with a CONFLO IV gas mixing system. Stable carbon isotope contents are given in per mil (‰) relative to the standard Vienna Pee Dee Belemnite (VPDB) with an external error better than ± 0.15‰. Radiocarbon (^{14}C-TOC) measurements were performed at the Biogeoscience laboratories and the Laboratory for Ion Beam Physics at ETH Zürich, Switzerland. Carbonates were removed by fumigation with HCl (37%, trace-metal purity) at 60°C for 72 h and samples measured on a coupled elemental analyzer-accelerator mass spectrometer (EA-AMS) system with a vario MICRO cube (Elementar, Germany) coupled to a Mini Carbon Dating System MICADAS (Ionplus, Switzerland) (e.g., Ruff et al., 2010). Radiocarbon values are reported in Δ^{14}C (‰) and ^{14}C-age as uncalibrated years (^{14}C yr).

Grain Size Analysis

Grain size of sediment particles was analyzed at AWI Potsdam following an established methodology (Schirrmeister et al., 2020). Organic material was removed by adding 100ml of 3% H_2O_2 over 3 to 6 weeks while on a shaking table. Organic-free sediments were then dispersed in 1L of water with dispersing agent (NH_4OH) in an overhead shaker to de-cluster particles.

Subsamples were then measured with a laser diffraction particle analyzer (Malvern Mastersizer 3000) with grain sizes measured between 0.375 to 1000 μm applying the Frauenhofer optical model. The cut-off value at 1000 μm was pre-set due to technical limitations of the particle analyzer.

Surface Area Analysis

Mineral surface area (SA) was measured to characterize the sediment structure of coastal debris. Approximately 1 g of subsampled sediment was combusted at 450°C for 12 h and rinsed with ultrapure water (MilliQ) to remove OC and salt, respectively. Afterwards, samples were freeze dried, degassed at 300°C with a vacuum applied for two hours and SA measured with a Nova 4200e SA analyzer (Quantachrome, United States) using the 6-point Brunauer–Emmett–Teller method (Brunauer et al., 1938).

Extraction and Analysis of Lipid Biomarkers

Lipid biomarkers (long-chain high molecular weight *n*-alkanes) were used to investigate the molecular composition of organic matter and its state of degradation (Eglinton and Hamilton, 1967). Lipid biomarkers were extracted at Vrije Universiteit Amsterdam, The Netherlands. Sediments (∼1 to 5 g) were extracted with a microwave digestion system MARS 6 (CEM, Germany) using dichloromethane (DCM) and methanol (MeOH) (9:1-volume ratio) at 100°C for 15 min. Microwave extracts were saponified with 10 ml potassium hydroxide (KOH, 0.5 M) in MeOH at 70°C for two hours. The neutral fraction was separated by wet-extraction with hexane following addition of 5 ml ultrapure water (MilliQ) with sodium chloride (NaCl). The neutral fraction was further separated into a-polar (containing the *n*-alkanes) and polar fractions by column chromatography using 5% deactivated silica (SiO_2). The *n*-alkanes were analyzed with a gas chromatograph mass spectrometer (GC-MS, Agilent, United States) at the Institute of Polar Sciences in Bologna, Italy. The GC temperature program started at 55°C followed by a ramp up of 4 to 5°C min^{-1} to a maximum temperature 300 to 310°C for 15 to 20 min. Lipid biomarker concentrations are given in μg g^{-1} TOC. In this study concentrations are reported in μg gdw^{-1} to use the same normalization as for cumulative CO_2 production.

Bulk and Molecular Degradation Proxies

We used several established proxies to assess the degradation state of organic matter. Molar TOC/TN-ratios (atomic ratio) and δ^{13}C-TOC values were used as general indicators for bulk organic matter origin, preservation and degradation state (Kuhry and Vitt, 1996; Lamb et al., 2006; Gundelwein et al., 2007).

A low TOC/TN-ratio or relative decrease indicates degradation with a preferential mineralization of TOC and immobilization of TN by microbes coupled to CO_2 release under aerobic conditions (Sollins et al., 1984; Stevenson, 1994; Strauss et al., 2015). High δ^{13}C-TOC values (enriched in ^{13}C, i.e., less negative values) indicate decomposition as organic matter degradation discriminates against the lighter carbon component (^{12}C), which results in a more negative δ^{13}C signature in the degrading fraction (Heyer et al., 1976; Strauss et al., 2015).

On a molecular level, we used the carbon preference index (CPI) for *n*-alkanes (ratio of odd over even-numbered C chain length homologues C_{22-34}) as indicator for the degree of microbial alteration of organic matter (Bray and Evans, 1961; Killops and Killops, 2004; Strauss et al., 2015). Living plants normally have CPI values greater 5 and decrease towards 1 with increasing maturity (Rielley et al., 1991; Vonk et al., 2010). High CPI values therefore indicate the presence of fresh organic matter, while mature or degraded organic matter displays lower CPI values. We further used high-molecular weight (HMW) to low-molecular weight (LMW) ratios of *n*-alkanes ($\Sigma C_{23-35}/\Sigma C_{14-19}$) as indicators for degradation since with ongoing degradation HMW compounds are broken down into LMW compounds (Killops and Killops, 2004). Additionally, we used the LMW-even to HMW-odd *n*-alkane ratio ($C_{16+18+20}/C_{27+29+31}$) with an increasing ratio indicating stronger microbial activity and degradation (Grimalt and Albaigés, 1987; Sánchez-García et al., 2014).

CO_2 Production and Model

The total CO_2 production (cum. CO_2 gdw^{-1}) over 60 days and daily production rates (μg CO_2 gdw^{-1} day^{-1}) give information on the magnitude and rates of initial aerobic TOC decomposition in a given sample and are commonly used as degradability indicators (e.g., Schädel et al., 2014). With the known total amount of CO_2 released we calculated the TOC loss in %.

CO_2 production was modeled four months and one year using an applied carbon decomposition model (Andrén and Kätterer, 1997; Knoblauch et al., 2013). The model is based on a first-order kinetic function, which reflects changes in OC content over time and considers how fast OC pools are being decomposed. Degradation rates were estimated using a non-linear least squares approach with an integrated trust-region-reflective algorithm in MATLAB (MathWorks, United States). The cumulative CO_2 production measured during the incubation was used to calibrate the model. A logarithmic transformation was applied to estimate decomposition time of OC for four months and an entire year.

RESULTS AND DISCUSSION

Organic Matter Origin and Composition

The composition of organic matter at the sampling sites was considerably different for most of the parameters considered (**Table 1**). The sediments at the investigated erosion sites mud lobe (n = 5) and cliff (n = 5) had TOC contents (1.4 ± 0.03 and 2.0 ± 0.4%), TOC/TN-ratios (10.2 ± 0.2 and 11.5 ± 0.5) and δ^{13}C concentrations (−25.8 ± 0.1 and −26.0 ± 0.2‰) typical for sediments containing terrestrial organic matter. Grain size structure was similar in both with the bulk of material (∼70 vol.%) composed of silt but was much more variable in the cliff (**Supplementary Figure 2**). The generally better sorting of mud lobe sediments may reflect hydrodynamic sorting during transport on land. The relatively high HMW/LMW *n*-alkane ratios ($\Sigma C_{23-35}/\Sigma C_{14-19}$) in mud lobe (17.7 ± 5.3) and cliff

(20.6 ± 9.3) samples indicated good preservation of wax lipids from terrestrial plant matter (Karlsson et al., 2015; Strauss et al., 2015). This is supported by a relatively high (close to 5) CPI for long-chain *n*-alkanes (C_{22-34}) in mud lobe and cliff sediments (4.6 ± 0.2 and 6.3 ± 0.9, respectively). The lower TOC/TN-ratios and $\delta^{13}C$ values in the mud lobe in combination with lower HMW/LMW ratios and CPI for *n*-alkanes indicated slightly more matured organic matter in the mud lobe and better preserved organic matter in the cliff. The ^{14}C-age of OC varied considerably between the sites with relatively old organic matter in the mud lobe (13,332 ± 2685 ^{14}C yr), most likely originating from deposition after the Wisconsin glaciation (Pollard, 1990; Fritz et al., 2012) and younger material in the cliff (5679 ± 1896 ^{14}C yr), which was potentially deposited during Holocene warm periods (Burn, 1997; Kaufman et al., 2009; Fritz et al., 2012).

The *mud debris* (MUD, $n = 1$) was a mixed sample of the mud lobe deposits and thus showed the same organic matter composition and ^{14}C-age (14,352 ^{14}C yr). Compared to the mud lobe this indicates its origin from thawed old permafrost, which was likely augmented by active layer material, melted massive ice and old slump floor deposits during transport (Lantuit and Pollard, 2005; Cray and Pollard, 2015; Tanski et al., 2017). Mineral SA of *mud debris* was 21.5 m^{-2} gdw^{-1}, reflecting the presence of fine-grained sediments in the silt and clay size fraction making up ∼72 and 17 vol.% (**Table 1**), respectively. In combination with relatively low TOC contents (1.5 wt%), the OC loading of *mud debris* was 0.7 mg OC m^{-2}. Collapsed active layer chunks from the slump headwall, which contained more modern and OC-rich sediments are usually (temporarily) deposited within the slump floor and mud lobe if not already transported offshore with the thaw stream draining the slump system (Kokelj et al., 2013; Tanski et al., 2017). During transport and mass wasting within the slump, a substantial portion of the organic matter was likely subject to degradation, resulting in the low TOC contents of the mud lobe and *mud debris* that was used in the incubation (Cray and Pollard, 2015; Tanski et al., 2017). This was supported by the much lower TOC content and TOC/TN-ratio (10.0) of the *mud debris* than the thaw slump headwall sediments (∼5 wt% and > 15, respectively; Tanski et al., 2017). These slump sediments were also characterized by the presence of fresh organic matter, reflected by CPI values for *n*-alkanes of close to 30 (Tanski et al., 2017).

The *cliff debris* (CD, $n = 1$) collected from the permafrost cliff toe was markedly different in its organic matter composition, both compared to the cliff itself and the *mud debris*. The relatively high TOC content (7.0 wt%) and TOC/TN-ratio (14.9) in combination with its younger ^{14}C-age of 2365 ^{14}C yr and higher $\delta^{13}C$ values of −26.0 ‰ indicate a strong contribution from relatively fresh and modern sources and C_3-plant material that accumulated in the *cliff debris* (Lamb et al., 2006). The mineral SA of *cliff debris* was 32.4 m^2 g^{-1} and silt and clay volumes ∼70 and 20 vol.%, respectively, indicating the presence of very fine-grained sediment fractions which in combination with high OC contents result in a high OC loading (2.1 mg OC m^{-2}). The relatively high CPI (5.5) as well as relatively high HMW/LMW ratios for *n*-alkanes (13.8) support the presence of relatively fresh organic matter in the *cliff debris* (Rielley et al., 1991; Strauss et al., 2015).

Constant vs. Rapid CO_2 Release

Considerable amounts of CO_2 were produced from *mud debris* and *cliff debris* over the two-months incubation period (**Figure 3** and **Table 2**). The total amount of CO_2 produced was significantly different (ANOVA, $p < 0.05$) between both, *mud debris* (**Figure 3A**) and *cliff debris* (**Figure 3B**), alongside with CO_2 production rates (**Supplementary Figure 3** and **Table 2**). *Mud debris* continuously released CO_2 at a relatively low rate with a maximum production of 50.6 ± 4.5 μg CO_2 gdw^{-1} day^{-1} at the beginning, which decreased to 14.0 ± 1.8 μg CO_2 gdw^{-1} day^{-1} at the end of the incubation, yielding a total of 1.4 ± 0.1 mg CO_2 gdw^{-1} over a period of two months (**Figure 3A**). Yet, when normalized to TOC content, the cumulative CO_2 production was almost three times higher from *mud debris* (93.4 ± 7.6 mg CO_2 g TOC^{-1}) compared to *cliff debris* (36.1 ± 12.7 mg CO_2 g TOC^{-1}). Outgassing of CO_2 from inorganic or petrogenic sources might have contributed to the observed CO_2 release as petrogenic OC is common in the study area and reactions of carbonates with sulphuric acid producing CO_2 were observed in thaw slump systems (Goñi et al., 2005; Drenzek et al., 2007; Zolkos et al., 2018). In contrast to the *mud debris*, *cliff debris* produced ca. three times more CO_2, adding up to a total amount of 4.0 ± 0.9 mg CO_2 gdw^{-1} over the two months of incubation, which was likely caused by the higher initial TOC content (7.0 wt%) and OC loading (2.1 mg OC m^{-2}; **Table 2** and **Figure 4**). CO_2 production rates were fairly high within the first month. Maximum rates observed were 154 ± 25.7 μg CO_2 gdw^{-1} day^{-1} and decreased to 34.2 ± 12.5 μg CO_2 gdw^{-1} day^{-1} after two months of incubation.

The total amount of CO_2 released from *mud debris* mixed with seawater was virtually the same per gram sediment (1.4 ± 0.1 mg CO_2 gdw^{-1}) and similar per g OC (96.4 ± 2.3 mg CO_2 g TOC^{-1}) as without seawater added. The CO_2 production rates were also similar with a maximum of 48.5 ± 4.9 μg CO_2 gdw^{-1} day^{-1} at the beginning (day 7) and 23.7 ± 1.4 μg CO_2 gdw^{-1} day^{-1} at the end of the incubation. The most labile OC compounds may have been mineralized and released already as CO_2 during transport *onshore* before transfer with the mud lobe to the ocean (Vonk et al., 2012; Abbott et al., 2014; Sánchez-García et al., 2014). For *cliff debris* mixed with seawater, however, the total amount of CO_2 produced was significantly higher (5.7 ± 0.4 mg CO_2 gdw^{-1}, ANOVA, $p < 0.05$), corresponding to ∼1.5 times more CO_2 released compared to without seawater added. This pattern was similar but less pronounced when normalized to g OC with 51.0 ± 6.0 mg CO_2 g TOC^{-1}. The set-ups with seawater resulted in elevated CO_2 production rates with a maximum of 328 ± 99.3 μg CO_2 gdw^{-1} day^{-1}. The production was particularly high during the first month, which likely indicates the rapid decomposition of freshly exposed and labile OC (Knoblauch et al., 2013; Schädel et al., 2014). The production rate then decreased to 29.5 ± 6.5 μg CO_2 gdw^{-1} day^{-1}, a similar value as for the set-up without seawater added. An increase in CO_2 production with addition of seawater was also observed in earlier studies for thawing permafrost from the thaw slump

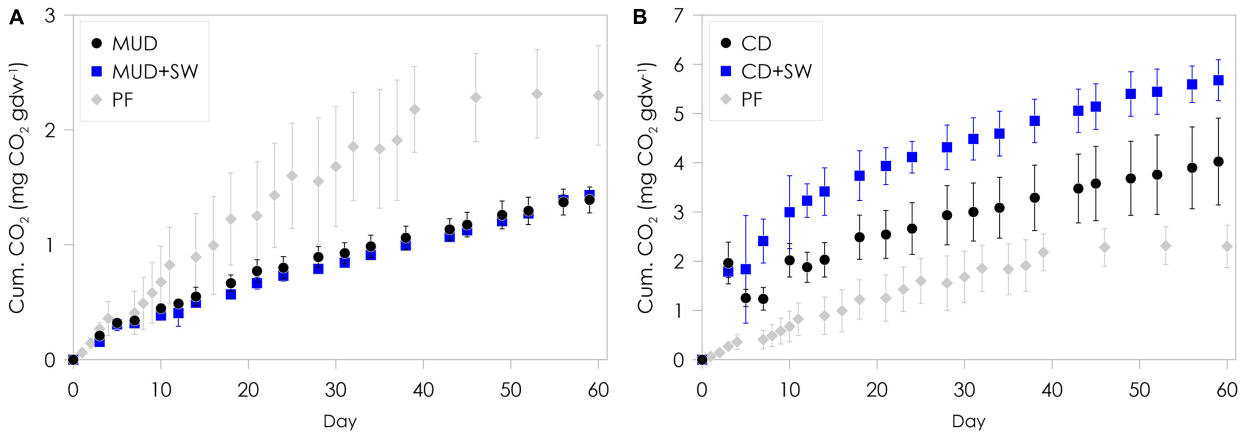

FIGURE 3 | Cumulative aerobic CO_2 production from incubated *mud debris* **(A)** and *cliff debris* **(B)**. *Mud debris* (MUD) and *cliff debris* (CD) were incubated without (black symbols) and with seawater (SW, blue symbols) for a duration of two months at 4°C under aerobic and dark conditions. Cumulative CO_2 production from permafrost (PF) is displayed as a local reference for CO_2 production from *in situ* permafrost without seawater (Tanski et al., 2019). The PF samples originate from the headwall of the thaw slump system from which the *mud debris* is released. The error bars show the standard deviation of the replicates used.

headwall, which might indicate a priming or co-metabolization effect (Bianchi, 2011; Tanski et al., 2019). Initial CO_2 production rates of *mud debris* were lower than those of *in situ* permafrost situated close to the sampling site in the thaw slump headwall (**Supplementary Figure 3**; Tanski et al., 2019). Yet, baseline production rates at the end of the two-month incubation period are slightly higher than from *in situ* permafrost. For *cliff debris,* initial as well as final CO_2 production rates were higher than for the permafrost reference site.

Following the CO_2 production in the first two months, the modeled CO_2 production and OC loss for the approximate length of the Arctic open-water season (∼four months) and an entire year, assuming that eroded sediments in the *nearshore zone* do not freeze-up anymore and that degradation is not only limited to the warm season, are substantially higher (**Table 2** and **Supplementary Figures 4, 5**). Model results explain ∼99% of the observed variations in CO_2 production for each individual sample and the residuals are usually unbiased and randomly scatter around zero. The only exceptions are residuals of cliff debris samples PI-14, PI-15 and PI-16 (**Supplementary Figure 5**), which show some pattern and hence should be dealt with cautiously. After four months, 2.7 ± 0.05 mg CO_2 gdw^{-1} would be released from mud debris *onshore*, corresponding to a TOC loss of $4.9 \pm 0.1\%$, which is slightly lower for set-ups with seawater added. The CO_2 release from *cliff debris onshore* would be 8.3 ± 0.8 mg CO_2 gdw^{-1} with TOC losses of $3.2 \pm 0.3\%$. This is also slightly lower when seawater is added. After one year upon erosion into the *nearshore*, *mud debris* would produce 6.1 ± 0.5 mg CO_2 gdw^{-1} with $11.1 \pm 0.9\%$ of the initial OC being lost. For *cliff debris* the CO_2 production would be much higher with 17.1 mg CO_2 gdw^{-1} corresponding to an OC loss of $6.9 \pm 1.7\%$. Model results based on set-ups without seawater show that the CO_2 release would be generally higher *onshore*. Yet, degradation is then limited to only ∼four months per year, making the erosion and year-round degradation of OC in the *nearshore* much more effective. On decadal timescales microbes would decompose the more refractory carbon pools and thus support further CO_2 production at low rates, adding to the cumulative release of CO_2 (Knoblauch et al., 2013; Schädel et al., 2014).

Experimental incubations that account for environmental conditions along eroding permafrost coastlines or continuous measurements of CO_2 or CH_4 from erosion sites are scarce in the Arctic, and our data are therefore challenging to put into context. GHG measurements are available from eroding permafrost cliffs at Muostakh Island (Siberian Arctic) with daily production rates ranging from 0.1 to 19.4 mg CO_2 m^{-2} day^{-1}, indicating intensive CO_2 release to the atmosphere in the warm season during erosion *onshore* (Vonk et al., 2012). For terrestrial permafrost sites elevated CO_2 concentrations of $>$ 1000 ppm were observed at thermoerosional features such as active layer detachment slides, gullies and thaw slumps, which also released substantial amounts of CH_4 (Abbott and Jones, 2015). These features might closely resemble the biogeochemical response of permafrost and modern OC to coastal erosion *onshore* as these processes are common along eroding coastlines as well (**Figures 1A,B**). Once eroded into coastal waters, permafrost OC rapidly settles due to ballasting within mineral matrices but may further degrade during resuspension and lateral transport, thus further producing CO_2 (Vonk et al., 2012, 2014; Semiletov et al., 2016; Bröder et al., 2018; Tanski et al., 2019; Jong et al., 2020).

Organic Matter Degradation vs. CO_2 Production

The release of CO_2 during the course of only two months indicates that organic matter is quickly degraded during the coastal erosion process. The production of CO_2 was positively correlated to TOC content and was higher in the OC-rich *cliff debris* than *mud debris* (**Figure 4A**), which implies that CO_2 release is likely a function of the availability of fresh and degradable organic matter. This is supported by strong

TABLE 2 | Summary of observed and modeled cumulative CO_2 production and corresponding TOC loss in % as CO_2-C after two months (60 days), regional open-water season of four months (120 days) and a full year (365 days) for incubation set-ups with *mud debris* (MUD), MUD with seawater (SW), *cliff debris* (CD) and CD with SW.

	MUD *n* = 5	MUD + SW *n* = 5	CD *n* = 3	CD + SW *n* = 3
Incubation (60 days)				
Cum. CO_2 prod. (mg gdw^{-1})	1.4 ± 0.1	1.4 ±0.03	4.0 ± 0.9	5.7 ±0.4
Cum. CO_2 prod. (mg g TOC^{-1})	93.4 ± 7.6	96.4 ±2.3	36.1 ± 12.7	51.0 ±6.0
Cum. CO_2 prod. (μg m^{-2})	62.9 ± 7.0	76.3 ±10.3	119.8 ± 26.2	195.3 ±15.0
TOC loss (% as CO_2-C)	2.5 ± 0.2	2.6 ±0.1	1.6 ± 0.3	2.2 ±0.2
Max. CO_2 prod. rate (μg gdw^{-1} day^{-1})	50.6 ± 4.5	48.5 ±4.9	153.7 ± 25.7	328.4 ±99.3
End CO_2 prod. rate (μg gdw^{-1} day^{-1})	14.0 ± 1.8	23.7 ±1.4	34.2 ± 12.5	29.5 ±6.5
Model (120 days)				
Cum. CO_2 prod. (mg gdw^{-1})	2.7 ± 0.05	2.3 ±0.1	8.3 ± 0.8	6.8 ±1.6
TOC loss (% as CO_2-C)	4.9 ± 0.1	4.3 ±0.2	3.2 ± 0.3	2.7 ±0.6
Model (365 days)				
Cum. CO_2 prod. (mg gdw^{-1})	7.8 ± 0.1	6.1 ±0.5	18.7 ± 2.1	17.7 ±4.3
TOC loss (% as CO_2-C)	14.3 ± 0.2	11.1 ±0.9	7.3 ± 0.8	6.9 ±1.7

Maximum and end daily CO_2 production rates are reported additionally. All values are given as mean ± standard deviation with the sample size (n).

correlations between CO_2 production and initial *n*-alkane CPI values and TOC/TN-ratio (**Figure 4E**, **Supplementary Figure 6** and **Table 1**). Yet, relative TOC losses (% as CO_2-C) were significantly smaller (ANOVA, $p < 0.05$) in *cliff debris* (1.6 ± 0.3%) compared to *mud debris* (2.5 ± 0.2%) (**Figure 4B**). In general, the lower initial TOC content seems to correlate weakly with a higher (relative) TOC loss, suggesting that the old and OC-poor *mud debris* might be more prone to degradation than the relatively young and OC-rich *cliff debris* despite the lower total CO_2 release. This is expressed by the higher CO_2 production per g OC in *mud debris* (93.4 ± 7.6 mg CO_2 g TOC^{-1}) compared to *cliff debris* (31.1 ± 12.7 mg CO_2 g TOC^{-1}) (**Figures 4**, **4C**). In contrast, CO_2 production is higher from *cliff debris* when normalized to SA (119.8 ± 26.2 μg CO_2 m^{-2}) compared to *mud debris* (62.9 ± 7.0 μg CO_2 m^{-2}) (**Figure 4D**) as the mineral OC-loading for *cliff debris* is higher than for *mud debris*. The production is even higher in set-ups with seawater added, particularly for *cliff debris* (195.3 ± 15.0 μg CO_2 m^{-2}) compared to *mud debris* (119.8 ± 26.2 μg CO_2 m^{-2}). The *cliff debris* site seems to be accumulating OC-rich fine-grained sediments with high OC content, mineral SA and clay portions, which finally result in the higher CO_2 release, whereas in the coarser *mud debris* this material may already have been removed offshore with the thaw stream or redeposited within the slump. With addition of seawater, CO_2 release from *cliff debris* increased, yet not significantly (ANOVA, $p < 0.05$), alongside with TOC losses (2.2 ± 0.2%), whereas for *mud debris* CO_2 production was similar for the set-ups with and without seawater added. Although the higher relative TOC losses from *mud debris* imply that it is more prone to degradation than the relatively young and OC-enriched *cliff debris*, the addition of seawater resulted in an increase of CO_2 production and corresponding TOC loss only in *cliff debris*. This might suggest that within *mud debris* the most labile compounds were already removed, and not available for further degradation in seawater. During transport within the slump system, this removal may have occurred via melting of massive ice that promoted leaching and liberation of more labile OC compounds and mineralization to CO_2 or CH_4 *onshore* (Vonk and Gustafsson, 2013; Abbott et al., 2014; Mann et al., 2015; Tanski et al., 2017). The relatively low mineral SA and OC loading of *mud debris* compared to *cliff debris* also suggest that the finer sediment fraction hosting OC may have been removed quickly from the *mud debris* with the thaw stream to the sea (Jong et al., 2020).

Incubated *mud debris* and *cliff debris* showed no significant changes in TOC contents, TOC/TN-ratios as well as in δ^{13}C-TOC and Δ^{14}C-TOC signatures (**Supplementary Figure 6**, **Table 1**). This is not surprising given the minor TOC losses (max. 2.5% of initial OC as CO_2-C) during these short-term incubations of two months, and considering measurement uncertainties and natural heterogeneity of organic matter in individual samples. On a molecular level, however, organic matter degradation seems to be more pronounced (**Figure 4**, **Supplementary Figure 7**, and **Table 1**). The CPI for *n*-alkanes decreased in all set-ups, indicating degradation of this organic matter fraction. In *mud debris* the CPI decreased from 4.6 ± 0.2 to 2.8 ± 0.3 and 2.4 ± 0.2 without and with seawater added, respectively (**Figure 4E**). This is similar, although less distinct, in *cliff debris*, where the CPI decreased from 5.5 to 3.5 ± 0.1 and 4.1 ± 0.5. Although the marked decrease of the HMW/LMW-ratio of *n*-alkanes mainly indicates the reworking of plant wax lipids (**Figure 4F**), the increase of LMW-even to HMW-odd *n*-alkanes (**Supplementary Figure 7**) support the overall degradation of organic matter (Sánchez-García et al., 2014). Yet, LMW and HMW *n*-alkane concentrations increased in all set-ups indicating *in situ* production processes during the course of the incubation (**Table 1** and **Supplementary Figure 8**). Therefore, the used degradation proxies cannot unambiguously reflect the OC degradation process as production probably distorts the signal.

The concentration increase of LMW and HMW *n*-alkanes was highest for set-ups without seawater added. In the incubated *mud debris*, *n*-alkane concentrations increased for LMW *n*-alkanes from 0.4 to 6.0 ± 1.0 (5.0 ± 0.9 μg gdw^{-1} when mixed with seawater) and for HMW *n*-alkanes from 7.6 to 18.5 ± 2.0 (15.5 ± 3.4 μg gdw^{-1} with seawater). In *cliff debris*, this pattern was similar with LMW *n*-alkane concentrations increasing from 0.5 to 8.0 ± 2.7 μg gdw^{-1} (6.6 ± 1.2 μg gdw^{-1} with seawater). For the HMW *n*-alkane concentrations, there were virtually no differences between set-ups with or without seawater added. Concentrations increased from 7.2 to 34.4 ± 4.2

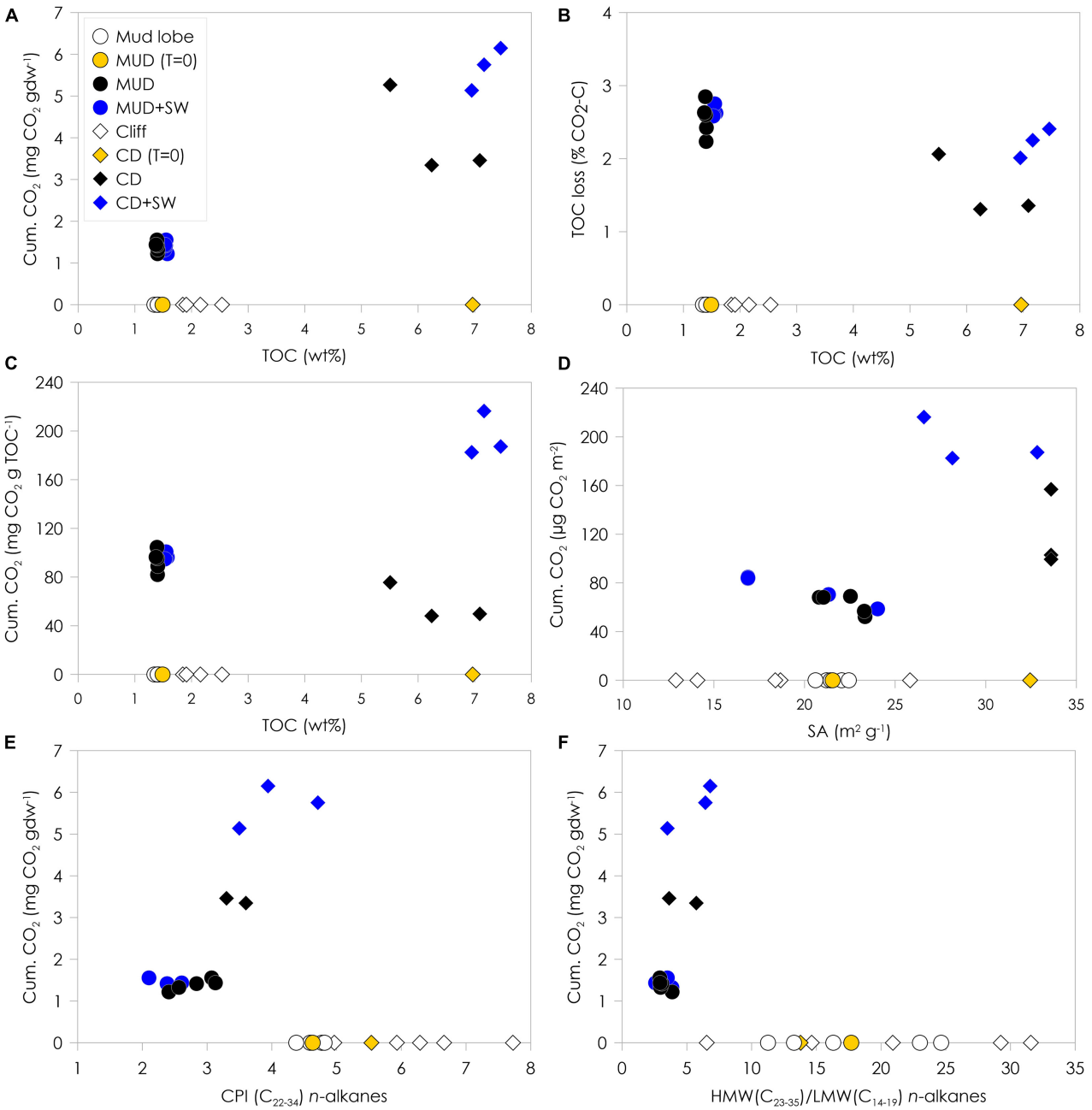

FIGURE 4 | Cumulative CO_2 production normalized to gram dry weight (gdw) and %TOC loss as CO_2-C at the end of the two month-incubation plotted against TOC content **(A,B)**, cumulative CO_2 production normalized to TOC content **(C)** and surface area **(D)** plotted against initial TOC content and surface area and cumulative CO_2 production normalized to gdw plotted against CPI *n*-alkanes **(E)** and HMW/LMW *n*-alkanes ratio **(F)**. Open symbols on the *x*-axis indicate samples from *mud lobe* and *cliff* that were not incubated to show the natural variability in the *mud lobe* and *cliff*. The *mud debris* (MUD) and *cliff debris* (CD) samples used for the incubation (T = 0) are indicated by the yellow symbols, incubated samples by the black symbols and incubated samples with seawater (SW) added by the blue symbols.

and 35.0 ± 5.1 µg gdw^{-1} with seawater added, respectively. While HMW *n*-alkane increase by up to four times during the incubation, LMW *n*-alkane concentrations increased up to 14 times compared to the initial concentrations (**Table 1**, **Supplementary Figure 9**). This substantial increase of *n*-alkanes under aerobic conditions, particularly LMW *n*-alkanes, may derive from heterotrophic microbial decomposers (Li et al., 2018; Chen et al., 2019). The predominance of even C-homologues in the LMW *n*-alkane fraction suggests a bacterial source and autochthonous production processes, which has been observed in estuarine and marine sediments (Grimalt and Albaigés, 1987). Under anoxic conditions, these LMW *n*-alkane C-homologues

can also derive from reduction of fatty acids (Debyser et al., 1977; Dastillung and Corbet, 1978). Yet, as aerobic conditions were applied during the experiment this process was probably restricted. Although no light was applied during the incubations, increases of LMW *n*-alkanes may have been also caused by algal growth as certain algae communities can thrive under extremely low radiance conditions (Suzuki et al., 1997). The lower even C-homologues in the HMW *n*-alkane fraction may point to the reduction of fatty acids or wax alcohols during degradation (Kvenvolden, 1970; Welte and Waples, 1973). Finally, contamination of lab equipment or by septa could also have been a potential source of *n*-alkanes. Yet, without further evidence the cause of the *n*-alkane increase remains speculative and biomarker from the post-incubation results should therefore be dealt with caution. However, the relatively low standard deviation of replicate analyses seems to rule out the random effect to be expected from septum leaching or contamination (**Supplementary Figure 9**).

DOC Release and Acidification

Over the course of the incubation, a minor portion of the sediment OC pool (< 0.2%) was transferred into the DOC pool of the seawater. After the incubation DOC concentrations in seawater increased from initial 1.7 ± 0.03 mg L^{-1} to 7.2 ± 0.1 mg L^{-1} and 27.8 ± 1.0 mg L^{-1} with addition of *mud debris* and *cliff debris,* respectively. The DOC increase in seawater mixed with *cliff debris* was ∼four times higher mainly due to the higher initial TOC content (**Supplementary Figure 10** and **Supplementary Table 2**). This higher DOC release probably resulted in the higher CO_2 release as OC has to be in the form of DOC to pass cell membranes before metabolization by microbes (Battin et al., 2008; Vonk and Gustafsson, 2013). Thus, when normalized to initial TOC content, DOC yields for *mud debris* and *cliff debris* after 2 month of incubation are similar with 3.1 ± 0.1 and 3.6 ± 0.1 mg g^{-1} OC, respectively. This indicates that DOC leaching and adsorption processes with mineral surfaces are of similar magnitude for both debris types during the two months of incubation (Neff and Asner, 2001; Littlefair et al., 2017). Higher DOC yields (6.6 ± 1.7 and 7.4 ± 1.4 mg g^{-1} OC, respectively) have been observed in seawater mixed with mineral and organic-rich permafrost in previous studies, where permafrost had similar initial TOC contents (1.7 ± 0.2 and 7.8 ± 0.7 wt%, respectively) to *mud debris* and *cliff debris,* yet the incubation period was twice as long (**Supplementary Figure 10**; Tanski et al., 2019). This suggests that leaching capacity and DOC yield may increase over time or that DOC components prone to leaching were already leached from *mud debris* and *cliff debris* during transport *onshore*. A dynamic balance of hydrolysis from particulate OC to DOC and subsequent mineralization into CO_2 was probably established within days (Kristensen et al., 1995). This is indicated by stabilization of CO_2 production rates after the initial CO_2 release during the first weeks stemming from rapid mineralization of the most labile compounds. Leaching of labile compounds from plant debris or mineral-bound OC is more likely for *cliff debris* since labile compounds were probably still available as transit time *onshore* until accumulation at the cliff toe was short (Dou et al., 2008; Blair and Aller, 2012; Vonk et al., 2015). In combination with the initial liberation of labile DOC compounds, priming and co-metabolization might have caused the initial increase of CO_2 production in *cliff debris* mixed with seawater (Bianchi, 2011). Input of additional nutrients with seawater might have promoted decomposition of organic matter (Mack et al., 2004). Furthermore, input of nutrients from the adjacent cliffs topsoil would have likely supported microbial metabolic efficiency in the *cliff debris* (Chen et al., 2018) and thus CO_2 production. The increase of DOC concentrations in unfiltered seawater controls from 1.7 ± 0.0 to 2.6 ± 1.0 mg L^{-1} (**Supplementary Table 2**) indicate potential production during the incubations and may support the increase of LMW *n*-alkanes observed. This could have further increased the DOC content in the seawater, which was mixed with *mud debris* and *cliff debris* and influences the CO_2 release from the seawater.

In combination with increasing DOC concentrations, a substantial acidification of the seawater mixed with *mud debris* and *cliff debris* from pH 8.2 to 7.0 ± 0.1 and 7.0 ± 0.0, respectively, was observed (**Supplementary Figure 10** and **Supplementary Table 2**). This could have been caused by a low pH of soil organic matter within eroded debris or dissolution of CO_2 produced from the debris in seawater. An even stronger pH decrease from 8.4 ± 0.1 to 5.2 ± 0.2, was observed during a longer incubation experiment with organic-rich permafrost mixed with seawater, which was likely caused by the low initial pH (6.1 ± 0.1) of the permafrost and a high DOC yield (**Supplementary Figure 10**; Tanski et al., 2019). Depending on the ratio of sediment to seawater, acidification could occur during erosion, which was shown for coastal waters in the Siberian Arctic that receive large amounts of permafrost OC. This, in turn, could result in elevated pCO_2 and outgassing to the atmosphere (Semiletov et al., 2013, 2016).

Incubations Cannot Account for Dynamic *in situ* Environmental Conditions

The measured CO_2 release rates and OC losses from eroded organic matter were obtained through experimental settings with low constant temperatures, maximum oxygen availability and dark conditions, which are classically used to study permafrost thaw through gradual active layer deepening (e.g., Lee et al., 2012; Knoblauch et al., 2013; Schädel et al., 2014). The CO_2 release observed under laboratory conditions would very likely differ from *in situ* observations. Yet, for coastal erosion processes onshore and in the nearshore coastal waters, environmental conditions are far from stable. The soil-to-water ratio under natural conditions is much lower resulting in a lower acidification as observed in the incubation vials. With a pH typical for ambient seawater (∼8.2), CO_2 production rates would probably remain similar but carbon storage in seawater would shift towards bicarbonate and carbonate (Wolf-Gladrow et al., 2007). The most important environmental parameters affecting the CO_2 production under natural conditions are most likely temperature and oxygen availability. Incubation experiments carried out at 15 or 16 °C (compared to 4 °C) showed that CO_2 production increased substantially compared to lower temperatures <4 °C

(Dutta et al., 2006; Lee et al., 2012; Knoblauch et al., 2013; Schädel et al., 2016; Tanski et al., 2019). For our study area Qikiqtaruk - Herschel Island temperatures in the coastal waters depend on wind direction and coastal orientation and range between ∼5 and 14°C during the warm season (Klein et al., 2019). This fits with observations from Cunliffe et al. (2019), which reported seawater surface temperatures between ∼6 to 10°C close to our sampling sites. During the warm season, air temperatures onshore are on average ∼8°C and soil temperatures in the active layer between 4.2 and 6.6°C with maximum values of 9.8°C (Burn, 2012; Wolter et al., 2016). The higher ambient temperatures would result in stronger OM mineralization rates onshore and in the nearshore under natural conditions compared to our incubation results. Using a Q10 value of 2 from Schädel et al. (2016), an average air temperature of ∼8°C, and a conservative seawater temperature of ∼6°C, the CO_2 production rates measured at 4°C would be ∼32% higher onshore at 8°C and ∼15% higher in the nearshore at 6°C. With warmer *in situ* seawater temperatures the solubility of CO_2 also decreases which further promotes the release of CO_2 to the atmosphere from coastal waters.

Another important driving factor for OC mineralization is the availability of oxygen. In contrast to the steady aerobic conditions during our incubation, which support efficient OC degradation and CO_2 production, less efficient anaerobic CO_2 and CH_4 production may apply onshore, where oxygen cannot penetrate deeper layers of the mud debris and cliff debris or under water-logged conditions. Under anaerobic conditions, OC mineralization is about 3 times slower than under aerobic conditions (Schädel et al., 2016; Knoblauch et al., 2018). This would result in an approximately three times lower theoretical OC loss of in mud debris and cliff debris (0.4 and 1.3%, respectively), where anaerobic conditions apply under natural condition, compared to the observed OC loss of 1.1 and 3.9%, respectively, under aerobic conditions in the experiment. In contrast to less efficient anaerobic mineralization of OM, drainage and drying of eroded material onshore could further increase oxygen penetration into eroded debris and support aerobic carbon mineralization. Inter or intra-annual refreezing cycles could further enhance macro-pore spaces and infiltration capacity of sediments (Ding et al., 2019). This could supply oxygen to pore spaces or further mechanical destruction of organo-mineral bonds, which may cause short-lived CO_2 pulses (Blair and Aller, 2012; Höfle et al., 2013; Walz et al., 2017). Additionally, drying and rewetting cycles (caused by rain, waves or high tides) could also further amplify CO_2 production by microbial mineralization of OC and weakening the physical protection of the soil matrix (Fierer and Schimel, 2003).

During transport onshore or in the nearshore water column, photo-oxidation can promote DOC degradation (by up to 40%), which is coupled to CO_2 release (Cory et al., 2013). The input of fresh nutrients, organic matter or plant litter from erosion itself, surface runoff or seawater could trigger priming effects and co-metabolism of recalcitrant organic matter combined from active layer and permafrost, thus further promoting CO_2 release (Abbott et al., 2014; Wild et al., 2014, 2016; Abbott and Jones, 2015; Walz et al., 2017; Knoblauch et al., 2018). Light conditions could further promote those priming effects in the ocean between produced algal exudates and eroded OC (Bianchi, 2011). The majority of these factors would likely lead to higher OC loss and CO_2 production under natural coastal erosion conditions compared to the experimental incubations set-ups employed in this study. Once deposited in nearshore sediments, OM degradation pathways depend on sedimentation rates and oxygen penetration depth. In our study region sedimentation rates range from 0.1 mm yr^{-1} offshore to 2 mm yr^{-1} in the vicinity of the Mackenzie River but can reach up to 0.33 cm yr^{-1} at shelf locations which promote deposition (Harper and Penland, 1982; Grotheer et al., 2020). In combination with an oxygen penetration depth of a few mm to cm in marine sediments (Glud, 2008; Arndt et al., 2013), we would assume that aerobic conditions similar as in our experiment would apply for eroded and deposited sediments within the first years of deposition and during resuspension, winnowing or longshore transport. In subsequent years, anaerobic conditions may gradually take over in the initially deposited sediments, limiting efficient OC degradation and promoting OC burial on geological time scales (Hilton et al., 2015; Bröder et al., 2018; Grotheer et al., 2020). Furthermore, due to competition with marine sulfate reduction, most likely no CH_4 would be produced in the marine surface sediments (Knoblauch et al., 2018).

CO_2 Release Dynamics Along the Yukon Coast

The erosion type and coastal morphology may strongly influence the GHG release potential along vulnerable permafrost coastlines. Our main study area, Qikiqtaruk – Herschel Island, is dominated by high cliffs (mean elevation ∼25 m) and retrogressive thaw slumps, which together affect ∼7% of the coast (**Figures 1**, **2**, Lantuit and Pollard, 2008; Ramage et al., 2017). Thermoabrasion of the cliff tops and headwall retreat in thaw slumps may result in an initial CO_2 pulse *onshore* with up to ∼4% of OC mineralized into CO_2 within one season (Tanski et al., 2019). Longer transport pathways of exposed organic matter along the sloping cliff faces or within thaw slump systems (**Figures 1A,B**) then result in a *delayed* release into the sea with further OC mineralization (∼5% OC loss as CO_2 measured during one warm season) at low rates (mimicked by *mud debris* incubations in this study) taking place in the subsequent warm seasons assuming the material discharges into the sea in the following years or even later. This adds to the initial permafrost CO_2 pulse *onshore* before release into the *nearshore* zone (**Figure 5**). Within thaw slump systems, eroded sediments can reside on long time scales *onshore* (years to decades) before release into the sea (Cray and Pollard, 2015). This long transit time can result in a substantial OC loss (up to ∼50%) with portions mineralized into CO_2 or CH_4 (Abbott et al., 2015; Tanski et al., 2017, 2019). Similarly, eroded debris can further accumulate on the beach for longer time spans (potentially exceeding one warm season) before being washed into the sea during storm surges or high tides (Obu et al., 2015; Cunliffe et al., 2019). This transition stage could further promote reworking of OC and direct CO_2 release to the atmosphere *onshore*. Photo-oxidation processes may have further increased degradation and

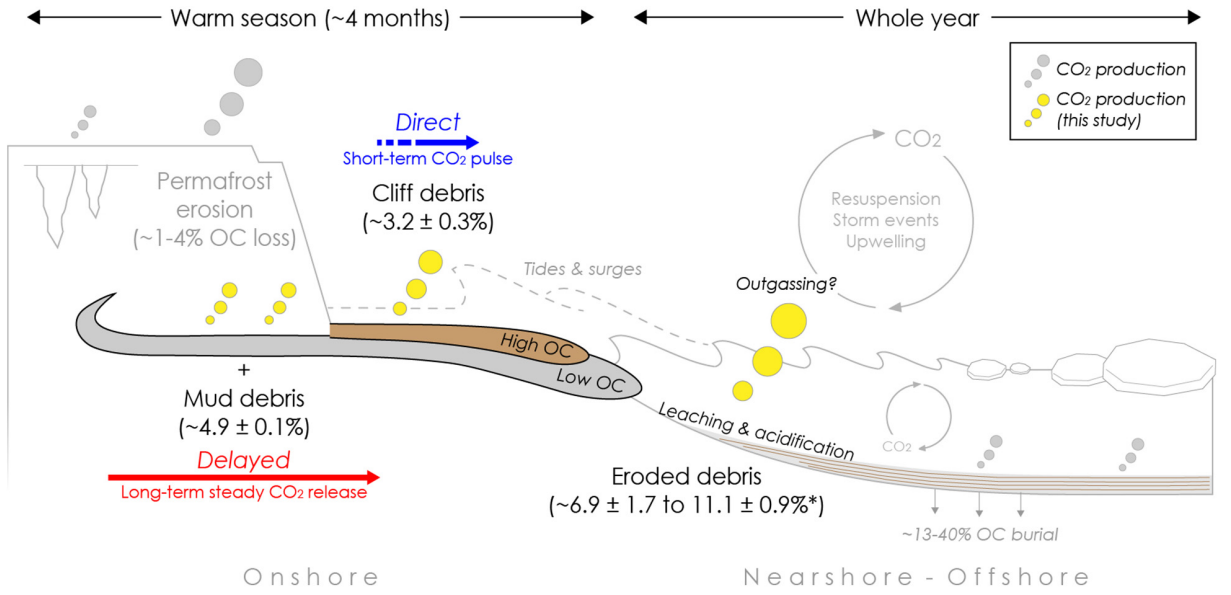

FIGURE 5 | Infographic summarizing potential organic carbon loss (%OC as CO_2) during coastal erosion processes from different erosion types in an Arctic warm season and entire year upon erosion in the sea. The magnitude of absolute carbon dioxide (mg CO_2 gdw) release is indicated by the size of yellow bubbles. Release of *mud debris* (gray flow) from thaw slumps or other thaw features into the *nearshore* is likely delayed with longer residence times *onshore,* resulting in a steady CO_2 release at low rates complementing CO_2 pulses during initial permafrost thaw and erosion. *Cliff debris* (brown flow) along low bluffs is likely to be transported more directly into the *nearshore,* resulting only in a short-term CO_2 pulse and overall low OC loss during transit (**Figure 1**). After erosion into the *nearshore* CO_2 is produced, which can be amplified by seawater, in particular for *cliff debris* and *in situ* permafrost where transport time is short. Carbon losses were modeled for the Arctic open-water season (~four months) and the entire year based on short term (~two months) incubation experiments at 4°C under dark and aerobic conditions. Carbon loss rates from permafrost erosion are taken from Tanski et al. (2019) and displayed as reference for *in situ* permafrost (~four month incubation at same conditions). The asterisk (*) indicates that once eroded into the sea OC degradation takes place during the entire year and is not limited to the warm seasons. Burial estimates are taken from Couture et al. (2018) and Grotheer et al. (2020).

CO_2 production during transit from land to sea (Cory et al., 2013; Ward and Cory, 2016).

In contrast, gully channels that intersect high bluffs, and thaw streams that drain slump systems (**Figures 1A,B**) may transport eroded permafrost OC more quickly and on a *direct* pathway towards the sea, potentially diminishing CO_2 release *onshore*. This *direct* pathway likely also applies to coastal stretches with low cliffs, which can be found especially on the southeast side of Qikiqtaruk – Herschel Island, which we tried to mimic with the *cliff debris* incubations. Along these cliffs (**Figures 2**, **5**), approximately 3% of OC can be mineralized into CO_2 within one warm season during transit *onshore*. The debris along low cliffs is likely removed quickly within one season with only larger collapsing permafrost blocks remaining for a longer period *onshore* on the beach (season to years). Correspondingly, the initial CO_2 pulse is likely complemented by continuing CO_2 production at lower rates. For this study we assumed aerated conditions during transport. Yet, when eroded material gets redeposited in mud pools or lobes *onshore*, CH_4 production may replace CO_2 production if water-logged and oxygen-depleted conditions apply (Knoblauch et al., 2013; Schädel et al., 2016).

Upon release into the *nearshore* waters, OC is likely further mineralized within erosion plumes or deposited sediments. Seawater may further promote OC mineralization (**Figure 5**), especially if transport is *direct* (in the case of collapsed permafrost or cliff debris) and if the water column is oxygen-saturated. Seawater enhances the CO_2 production from *cliff debris* with corresponding OC losses increasing from 1.6 ± 0.3 to 2.2 ± 0.2% after incubation with seawater mimicking *nearshore* conditions (**Table 2**). Enhanced OC loss was also observed for *in situ* permafrost mixed with seawater with TOC losses increasing from 1.1 ± 0.0 to 1.5 ± 0.2% in organic-rich permafrost and from 3.9 ± 0.2 to 6.2 ± 1.2% in mineral permafrost (Tanski et al., 2019). If transport to the *nearshore* is *delayed*, OC transferred to the sea probably continues to degrade at the same relatively low rates as *onshore* with OC losses of ~5% within a warm season of four months (**Figure 5**). Yet, for both scenarios organic matter degradation in *nearshore* sediments likely takes place during the entire year and is not limited only to the warm season since *nearshore* sediments do not freeze up during the cold season. Once eroded into the *nearshore*, the total OC loss as CO_2-C from *mud debris* and *cliff debris* could be ~7–11% after one year (**Figure 5**). Depending on the depositional environment, OC can be either buried on the shelf or transported towards the continental slope on up to millennial time scales (Naidu et al., 2000; Goñi et al., 2013; Bröder et al., 2018). Locally, large portions of eroded OC (~12 to 40%) are stored in *nearshore* sediments and local depressions on the shelf such as Herschel Basin (Couture et al., 2018; Grotheer et al., 2020). On the seafloor, effective aerobic degradation likely only takes place in the upper few millimeters of the sediment column and at the water-sediment boundary, where microbial communities allow

for higher respiration rates (Rasmussen and Jorgensen, 1992; Arndt et al., 2013; Brüchert et al., 2018). Bioturbation, currents and ice scouring may facilitate resuspension and therefore oxygen resupply and CO_2 production in deeper sediment columns eventually (Héquette et al., 1995; Arndt et al., 2013). Under anaerobic conditions microbial communities that can produce CH_4 can establish after years and substantial amounts of CH_4 being produced and released either directly as CH_4 or oxidized as CO_2 from the seafloor (Overduin et al., 2015; Knoblauch et al., 2018). Although further GHG production of eroded material is very likely in the *nearshore*, it is unclear if or from which water depth produced CO_2 evades to the atmosphere. Outgassing of degradation-derived CO_2 or CH_4 from oversaturated water layers, however, can occur locally and is promoted by resuspension, storms or upwelling events (Mathis et al., 2012; Vonk et al., 2012; Semiletov et al., 2016; Pipko et al., 2017).

Along the adjacent Yukon mainland coast approximately one third of the entire coastline is characterized by actively eroding cliffs (of variable elevation), with the remainder being gently sloping tundra (∼17%) and inundated coastlines (∼11%) as well as beach and gravel spits (Irrgang et al., 2018). A *delayed* release similar to the high cliffs on Qikiqtaruk – Herschel Island may apply to the actively eroding cliffs in the formerly glaciated part of the Yukon coast towards the Mackenzie Delta. Here, cliffs are high (mean elevation of up to ∼30m) and thaw slumps are ubiquitous (up to ∼16% of the coastline) promoting substantial OC turnover *onshore* before release into the ocean (Couture and Pollard, 2015; Ramage et al., 2017). In the formerly unglaciated part towards the Alaskan border (**Figures 1C,D**), cliffs are much lower (∼6.5 m mean elevation) and residence times of eroded OC *onshore* likely to be very short (weeks to years) due to the particularly high erosion rates in this region (∼1.4 m yr^{-1}), which results in a shorter time span for OC mineralization during erosion (Couture and Pollard, 2015; Irrgang et al., 2018). Along coastal parts where tundra is sloping towards the beach and thereby restricting exposure of permafrost, OC loss might be even lower and the cycling of released OC may primarily take place in the seawater column or upon deposition in *nearshore* sediments. In turn, inundation and potential permafrost degradation could promote OC mineralization *onshore* and release substantial amounts of CO_2 before transport into the ocean (Tanski et al., 2019). At present, how much OC is converted into CO_2 along the different coastal types is highly speculative. Yet, it is likely that the response of OC to erosion and the magnitude of CO_2 release varies between coastal and erosion types. Based on the annual TOC flux from land to sea of 36 Gg yr^{-1} for the Yukon coast (Couture et al., 2018), we would estimate that up to 1.8 Gg CO_2 yr^{-1} could be released as CO_2 during the erosion process onshore assuming an OC loss of up to ∼5% during the warm season and up to 3.9 Gg CO_2 yr^{-1} from *nearshore* sediments assuming an OC loss of ∼11% for an entire year since eroded sediments on the seafloor do not freeze anymore (**Figure 5**). Local dynamic environmental conditions (e.g., higher air temperatures and sunlight exposure) and processes (e.g., drying and rewetting of debris in the coastal zone) may increase OC degradation.

CONCLUSION

Coastal morphology and erosion type play a substantial role in determining the greenhouse gas release potential during erosion along permafrost coasts in the Arctic. *Mud debris* and *cliff debris* from an outflow of a thaw slump system and a low collapsing bluff, respectively, representing different coastal erosion scenarios released substantial amounts of CO_2 (1.4 ± 0.1 to 4.0 ± 0.9 mg CO_2 gdw^{-1}) over a short period (∼two months) corresponding to an initial OC loss ∼1.6–2.6%. The relatively fresh and OC-rich *cliff debris* resulted in a ∼four times higher CO_2 release than for *mud debris*. Yet, when normalized to OC content, CO_2 release was ∼three times higher from *mud debris* indicating higher biodegradability of the older and more mineral OC. CO_2 release was particularly high with addition of seawater, indicating potential priming effects in the coastal realm. Upon release into the ocean, only a small portion of OC initially enters the seawater DOC pool. Our results suggest that high bluffs or coasts with presence of thermoerosional features are characterized by a *delayed* release that consists of an initial CO_2 pulse from permafrost erosion followed by a subsequent CO_2 release at lower rates in *mud debris*, promoting OC degradation during protracted transit from land to sea in the warm season. In contrast, erosion of *cliff debris* along low bluffs that may contain proportionally more OC results only in a short-term CO_2 pulse with OC quickly removed by waves. In the *nearshore* zone, CO_2 production from eroded sediments continues provided oxygen is available, likely taking place the entire year. After the duration of an Arctic warms season (∼four month) OC losses of up ∼5% were modeled and after one year, up to ∼11% of OC could be decomposed and released as CO_2 once eroded sediments are deposited in the *nearshore*. The magnitude of CO_2 release may be underestimated when using traditional incubation experiments since coastal environmental conditions are difficult to account for yet likely enhance degradation. More sophisticated incubation set-ups that mimic changing environmental and site-specific variables, or continuous GHG measurement systems *onshore* (e.g., eddy covariance towers) and in the *nearshore* (e.g., pop-up buoys with *in situ* pCO_2 sensors), accounting for seasonal fluctuations and uptake processes from vegetation and phytoplankton, would be needed to derive the actual GHG release signal along eroding permafrost coasts in different Arctic regions.

DATA AVAILABILITY STATEMENT

The raw data supporting the conclusions of this article will be made available by the authors, without undue reservation.

AUTHOR CONTRIBUTIONS

GT, HL, DW, JV, and LB created the study design and incubation set-up. GT, DW, and TS carried out the gas concentration measurements. CK and GT recalculated gas concentration and estimated TOC losses. CB calibrated and applied the dynamic

carbon decomposition model. GT and LB carried out the extraction of lipid biomarkers. TT measured lipid biomarkers. LB, JV, GT, and TT processed and interpreted the data. HL, MF, and JS supported the bulk geochemical and stable carbon isotope analysis and data interpretation. BK measured and evaluated DOC concentrations. LB, NH, and TE carried out radiocarbon analysis and data analysis. GT wrote the manuscript with contributions from all co-authors. All authors contributed to the article and approved the submitted version.

FUNDING

We acknowledge and are grateful for the financial support from the H2020 project NUNATARYUK (grant 773421), the Helmholtz young investigators group TEAM (grant VH-NG-821 to TS) and the ERC StG project THAWSOME (grant 676982 to JV). JS was supported by the Changing Arctic Ocean program (NERC-BMBF project CACOON, grant 03F0806A) and CB by the German research foundation DFG (BE 6485/1-1).

ACKNOWLEDGMENTS

We would like to thank O. Burckhardt, J. Oury, C. Burau, D. Scheidemann, H. Meyer, M. Weiner, K. Keskitalo, and D. Jong for support during lab work. K. Klein and D. Jong are thanked for assistance during field work and J. Kahl for logistical support. We thank A. Irrgang for contributing photographs from field work. We would like to especially thank the park rangers and R. Gordon from Qikiqtaruk – Herschel Island Territorial Park for their support and guidance on their land. The Aurora Research Institute in Inuvik is thanked for the logistical support on site. Data supporting this study is available on the PANGAEA data repository (in review; data submitted on 05 January 2021).

SUPPLEMENTARY MATERIAL

The Supplementary Material for this article can be found online at: https://www.frontiersin.org/articles/10.3389/feart.2021.630493/full#supplementary-material

REFERENCES

Abbott, B. W., and Jones, J. B. (2015). Permafrost collapse alters soil carbon stocks, respiration, CH4, and N2O in upland tundra. *Glob. Change Biol.* 21, 4570–4587. doi: 10.1111/gcb.13069

Abbott, B. W., Jones, J. B., Godsey, S. E., Larouche, J. R., and Bowden, W. B. (2015). Patterns and persistence of hydrologic carbon and nutrient export from collapsing upland permafrost. *Biogeosciences* 12, 3725–3740. doi: 10.5194/bg-12-3725-2015

Abbott, B. W., Larouche, J. R., Jones, J. B., Bowden, W. B., and Balser, A. W. (2014). Elevated dissolved organic carbon biodegradability from thawing and collapsing permafrost. *J. Geophys. Res. Biogeosci.* 119, 2049–2063. doi: 10.1002/2014JG002678

AMAP (2017). *Snow, Water, Ice and Permafrost in the Arctic (SWIPA) 2017*. Oslo: Arctic Monitoring and Assessment Programme.

Andrén, O., and Kätterer, T. (1997). ICBM: the introductory carbon balance model for exploration of soil carbon balances. *Ecol. Appl.* 7, 1226–1236. doi: 10.1890/1051-07611997007[1226:ITICBM]2.0.CO;2

Are, F. E., Reimnitz, E., Grigoriev, M. N., Hubberten, H. W., and Rachold, V. (2008). The influence of cryogenic processes on the erosional arctic shoreface. *J. Coast. Res.* 241, 110–121. doi: 10.2112/05-0573.1

Arndt, S., Jørgensen, B. B., LaRowe, D. E., Middelburg, J. J., Pancost, R. D., and Regnier, P. (2013). Quantifying the degradation of organic matter in marine sediments: a review and synthesis. *Earth Sci. Rev.* 123, 53–86. doi: 10.1016/j.earscirev.2013.02.008

Barnhart, K. R., Anderson, R. S., Overeem, I., Wobus, C., Clow, G. D., and Urban, F. E. (2014). Modeling erosion of ice-rich permafrost bluffs along the Alaskan Beaufort Sea coast. *J. Geophys. Res. Earth Surf.* 119, 1155–1179. doi: 10.1002/2013JF002845

Battin, T. J., Kaplan, L. A., Findlay, S., Hopkinson, C. S., Marti, E., and Packman, A. I. (2008). Biophysical controls on organic carbon fluxes in fluvial networks. *Nat. Geosci.* 1, 95–100. doi: 10.1038/ngeo101

Bendixen, M., Iversen, L. L., Bjørk, A. A., Elberling, B., Westergaard-Nielsen, A., Overeem, I., et al. (2017). Delta progradation in Greenland driven by increasing glacial mass loss. *Nature* 550, 101–104. doi: 10.1038/nature23873

Bianchi, T. S. (2011). The role of terrestrially derived organic carbon in the coastal ocean: a changing paradigm and the priming effect. *Proc. Natl. Acad. Sci. U.S.A.* 108, 19473–19481. doi: 10.1073/pnas.1017982108

Biskaborn, B. K., Smith, S. S., Noetzli, J., Matthes, H., Vieira, G., Streletskiy, D. A., et al. (2019). Permafrost is warming at a global scale. *Nat. Commun.* 10:264. doi: 10.1038/s41467-018-08240-4

Blair, N., and Aller, R. (2012). The fate of terrestrial organic carbon in the marine environment. *Annu. Rev. Mar. Sci.* 4, 401–423. doi: 10.1146/annurev-marine-120709-142717

Blasco, S. M., Fortin, G., Hill, P. R., O'Connor, M. J., and Brigham-Grette, J. K. (1990). "The late neogene and quaternary stratigraphy of the Canadian Beaufort continental shelf," in *The Arctic Ocean Region*, eds A. Grantz, L. Johnson, and J. F. Sweeney (Boulder, CO: Geological Society of America), 491–502.

Bray, E. E., and Evans, E. D. (1961). Distribution of n-paraffins as a clue to recognition of source beds. *Geochim. Cosmochim. Acta* 22, 2–15. doi: 10.1016/0016-7037(61)90069-2

Bröder, L., Tesi, T., Andersson, A., Semiletov, I., and Gustafsson, Ö (2018). Bounding cross-shelf transport time and degradation in Siberian-Arctic land-ocean carbon transfer. *Nat. Commun.* 9:806. doi: 10.1038/s41467-018-03192-1

Brüchert, V., Bröder, L., Sawicka, J. E., Tesi, T., Joye, S. P., Sun, X., et al. (2018). Carbon mineralization in Laptev and East Siberian sea shelf and slope sediment. *Biogeosciences* 15, 471–490. doi: 10.5194/bg-15-471-2018

Brunauer, S., Emmett, P. H., and Teller, E. (1938). Adsorption of gases in multimolecular layers. *J. Am. Chem. Soc.* 60, 309–319. doi: 10.1021/ja01269a023

Burn, C. R. (1997). Cryostratigraphy, paleogeography, and climate change during the early Holocene warm interval, western Arctic coast, Canada. *Can. J. Earth Sci.* 34, 912–925. doi: 10.1139/e17-076

Burn, C. R. (2012). *Herschel Island Qikiqtaryuk - A Natural and Cultural History of Yukon's Arctic Island*. Calgary: University of Calgary Press.

Burn, C. R., and Zhang, Y. (2009). Permafrost and climate change at Herschel Island (Qikiqtaruq), Yukon Territory, Canada. *J. Geophys. Res. Earth Surf.* 114, 1–16. doi: 10.1029/2008JF001087

Chen, L., Liu, L., Mao, C., Qin, S., Wang, J., Liu, F., et al. (2018). Nitrogen availability regulates topsoil carbon dynamics after permafrost thaw by altering microbial metabolic efficiency. *Nat. Commun.* 9:3951. doi: 10.1038/s41467-018-06232-y

Chen, X., Liu, X., Wei, Y., and Huang, Y. (2019). Production of long-chain n-alkyl lipids by heterotrophic microbes: new evidence from Antarctic lakes. *Organ. Geochem.* 138:103909. doi: 10.1016/j.orggeochem.2019.103909

Ciais, P., Sabine, C., Bala, G., Bopp, L., Brovkin, V., Canadell, J., et al. (eds) (2013). "Carbon and other biogeochemical cycles," in *Climate Change 2013: The Physical Science Basis. Contribution of Working Group 1 to the Fifth Assessment Report of the Intergovernmental Panel on Climate Change*, eds T. F. Stocker, D. Qin, G. K. Plattner, M. Tignor, S. K. Allen, J. Boschung, et al. (Cambridge: Cambridge University Press).

Coch, C., Lamoureux, S. F., Knoblauch, C., Eischeid, I., Fritz, M., Obu, J., et al. (2018). Summer rainfall dissolved organic carbon, solute, and sediment fluxes in

a small Arctic coastal catchment on Herschel Island (Yukon Territory, Canada). *Arct. Sci.* 4, 750–780. doi: 10.1139/as-2018-0010

Cory, R. M., Crump, B. C., Dobkowski, J. A., and Kling, G. W. (2013). Surface exposure to sunlight stimulates CO2 release from permafrost soil carbon in the Arctic. *Proc. Natl. Acad. Sci. U.S.A.* 110, 3429–3434. doi: 10.1073/pnas.1214104110

Couture, N., and Pollard, W. H. (2015). "Ground ice determinations along the Yukon coast using a morphological model," in *Proceedings, GeoQuebec 2015, 7th Canadian Permafrost Conference*, (Québec).

Couture, N. J., Irrgang, A., Pollard, W., Lantuit, H., and Fritz, M. (2018). Coastal erosion of permafrost soils along the Yukon coastal plain and fluxes of organic carbon to the Canadian Beaufort Sea. *J. Geophys. Res. Biogeosci.* 123, 406–422. doi: 10.1002/2017JG004166

Cray, H., and Pollard, W. H. (2015). Vegetation recovery patterns following permafrost disturbance in a low arctic vegetation recovery patterns following permafrost disturbance in a low arctic setting: case study of Herschel Island, Yukon, Canada. *Arct. Antarct. Alpine Res.* 47, 99–113. doi: 10.1657/AAAR0013-076

Cunliffe, A. M., Tanski, G., Radosavljevic, B., Palmer, W. F., Sachs, T., Lantuit, H., et al. (2019). Rapid retreat of permafrost coastline observed with aerial drone photogrammetry. *Cryosphere* 13, 1513–1528.

Dai, A., Luo, D., Song, M., and Liu, J. (2019). Arctic amplification is caused by sea-ice loss under increasing CO2. *Nat. Commun.* 10:121. doi: 10.1038/s41467-018-07954-9

Dastillung, M., and Corbet, B. (1978). "La geochimie organique des sediments marins profonds. I: hydrocarbures satures et insatures des sediments," in *Geochimie Organique Des Sediments Marins Profonds*, eds A. Cabanaz and R. Pelet (Paris: CNRS), 293–323.

Debyser, Y., Pelet, R., and Dastillung, M. (1977). "Geochimie organique des sediments marins recents: Mer Noire, Baltique, Atlantique (Mauritanie)," in *Advanes in Organic Geohemistry*, eds R. Campos and J. Goni (Madrid: Empresa Nacional Adaro de Investigaciones Mineras), 289–320.

Ding, B., Rezanezhad, F., Gharedaghloo, B., Van Cappellen, P., and Passeport, E. (2019). Bioretention cells under cold climate conditions: Effects of freezing and thawing on water infiltration, soil structure, and nutrient removal. *Sci. Total Environ.* 649, 749–759. doi: 10.1016/j.scitotenv.2018.08.366

Dou, F., Ping, C.-L., Guo, L., and Jorgenson, T. (2008). Estimating the impact of seawater on the production of soil water-extractable organic carbon during coastal erosion. *J. Environ. Qual.* 37, 2368–2374. doi: 10.2134/jeq2007.0403

Drenzek, N. J., Montluçon, D. B., Yunker, M. B., Macdonald, R. W., and Eglinton, T. I. (2007). Constraints on the origin of sedimentary organic carbon in the Beaufort Sea from coupled molecular 13C and 14C measurements. *Mar. Chem.* 103, 146–162. doi: 10.1016/j.marchem.2006.06.017

Dunton, K. H., Weingartner, T., and Carmack, E. C. (2006). The nearshore western Beaufort Sea ecosystem: circulation and importance of terrestrial carbon in arctic coastal food webs. *Prog. Oceanogr.* 71, 362–378. doi: 10.1016/j.pocean.2006.09.011

Dutta, K., Schuur, E. A. G., Neff, J. C., and Zimov, S. A. (2006). Potential carbon release from permafrost soils of Northeastern Siberia. *Glob. Change Biol.* 12, 2336–2351. doi: 10.1111/j.1365-2486.2006.01259.x

Eglinton, G., and Hamilton, R. J. (1967). Leaf epicuticular waxes. *Science* 156, 1322–1334. doi: 10.2307/1721263

Fierer, N., and Schimel, J. P. (2003). A proposed mechanism for the pulse in carbon dioxide production commonly observed following the rapid rewetting of a dry soil. *Soil Sci. Soc. Am. J.* 67, 798–805. doi: 10.2136/SSSAJ2003.7980

Forbes, D. (2019). "Chapter 8 - Arctic deltas and estuaries: a canadian perspective," in *Coasts and Estuaries The Future*, eds E. Wolanski, J. W. Day, M. Ellitt, and R. Ramachadran (Amsterdam: Elsevier).

Fritz, M., Vonk, J. E., and Lantuit, H. (2017). Collapsing arctic coastlines. *Nat. Clim. Change* 7, 6–7. doi: 10.1038/nclimate3188

Fritz, M., Wetterich, S., Schirrmeister, L., Meyer, H., Lantuit, H., Preusser, F., et al. (2012). Eastern Beringia and beyond: late Wisconsinan and Holocene landscape dynamics along the Yukon Coastal Plain, Canada. *Palaeogeogr. Palaeoclimatol. Palaeoecol.* 319–320, 28–45. doi: 10.1016/j.palaeo.2011.12.015

Glud, R. (2008). Oxygen dynamics of marine sediments. *Mar. Biol. Res.* 4, 243–289. doi: 10.1080/17451000801888726

Goñi, M. A., O'Connor, A. E., Kuzyk, Z. Z., Yunker, M. B., Gobeil, C., and Macdonald, R. W. (2013). Distribution and sources of organic matter in surface marine sediments across the North American Arctic margin. *J. Geophys. Res. Oceans* 118, 4017–4035. doi: 10.1002/jgrc.20286

Goñi, M. A., Yunker, M. B., Macdonald, R. W., and Eglinton, T. I. (2005). The supply and preservation of ancient and modern components of organic carbon in the Canadian Beaufort Shelf of the Arctic Ocean. *Mar. Chem.* 93, 53–73. doi: 10.1016/j.marchem.2004.08.001

Grimalt, J., and Albaigés, J. (1987). Sources and occurrence of C12C22 n-alkane distributions with even carbon-number preference in sedimentary environments. *Geochim. Cosmochim. Acta* 51, 1379–1384. doi: 10.1016/0016-7037(87)90322-X

Grotheer, H., Meyer, V., Riedel, T., Pfalz, G., Mathieu, L., Hefter, J., et al. (2020). Burial and origin of permafrost-derived carbon in the nearshore zone of the Southern Canadian Beaufort Sea. *Geophys. Res. Lett.* 47:e2019GL085897. doi: 10.1029/2019GL085897

Gundelwein, A., Müller-Lupp, T., Sommerkorn, M., Haupt, E. T. K., Pfeiffer, E. M., and Wiechmann, H. (2007). Carbon in tundra soils in the Lake Labaz region of arctic Siberia. *Eur. J. Soil Sci.* 58, 1164–1174. doi: 10.1111/j.1365-2389.2007.00908.x

Günther, F., Overduin, P. P., Sandakov, A. V., Grosse, G., and Grigoriev, M. N. (2013). Short- and long-term thermo-erosion of ice-rich permafrost coasts in the Laptev Sea region. *Biogeosciences* 10, 4297–4318. doi: 10.5194/bg-10-4297-2013

Günther, F., Overduin, P. P., Yakshina, I. A., Opel, T., Baranskaya, A. V., and Grigoriev, M. N. (2015). Observing Muostakh disappear: permafrost thaw subsidence and erosion of a ground-ice-rich Island in response to arctic summer warming and sea ice reduction. *Cryosphere* 9, 151–178. doi: 10.5194/tc-9-151-2015

Harper, J. R., and Penland, P. S. (1982). *Beaufort Sea Sediment Dynamics. Contract Report to Atlantic Geoscience Centre*. Ottawa, ON: Geological Survey of Canada.

Hequette, A., and Barnes, P. W. (1990). Coastal retreat and shoreface profile variations in the Canadian Beaufort Sea. *Mar. Geol.* 91, 113–132. doi: 10.1016/0025-3227(90)90136-8

Héquette, A., Desrosiers, M., and Barnes, P. W. (1995). Sea ice scouring on the inner shelf of the southeastern Canadian Beaufort Sea. *Mar. Geol.* 128, 201–219. doi: 10.1016/0025-3227(95)00095-G

Heslop, J. K., Chandra, S., Sobzcak, W. V., Davydov, S. P., Davydova, A. I., Spektor, V. V., et al. (2017). Variable respiration rates of incubated permafrost soil extracts from the Kolyma River lowlands, north-east Siberia. *Polar Res.* 37:1305157. doi: 10.1080/17518369.2017.1305157

Heyer, J., Hübner, H., and Maaβ, I. (1976). Isotopenfraktionierung des Kohlenstoffs bei der mikrobiellen Methanbildung. *Isotopenpraxis Isotop. Environ. Health Stud.* 12, 202–205. doi: 10.1080/10256017608543912

Hilton, R. G., Galy, V., Gaillardet, J., Dellinger, M., Bryant, C., et al. (2015). Erosion of organic carbon in the Arctic as a geological carbon dioxide sink. *Nature* 524, 84–87. doi: 10.1038/nature14653

Höfle, S., Rethemeyer, J., Mueller, C. W., and John, S. (2013). Organic matter composition and stabilization in a polygonal tundra soil of the Lena Delta. *Biogeosciences* 10, 3145–3158. doi: 10.5194/bg-10-3145-2013

Hugelius, G., Strauss, J., Zubrzycki, S., Harden, J. W., Schuur, E. A. G., Ping, C. L., et al. (2014). Estimated stocks of circumpolar permafrost carbon with quantified uncertainty ranges and identified data gaps. *Biogeosciences* 11, 6573–6593. doi: 10.5194/bg-11-6573-2014

Huggett, W. S., Woodward, M. J., Stephenson, F., Hermiston, F. V., and Douglas, A. (1975). *Near and Bottom Currents and Offshore Tides, Ocean and Aquatic Sciences, Beaufort Sea Technical Report No. 16*. Victoria, BC: Ocean and Aquatic Sciences Department of the Environment.

Irrgang, A. M., Lantuit, H., Manson, G. K., Günther, F., Grosse, G., and Overduin, P. P. (2018). Variability in rates of coastal change along the Yukon Coast, 1951 to 2015. *J. Geophys. Res. Earth Surf.* 123, 779–800. doi: 10.1002/2017JF004326

James, T. S., Henton, J. A., Leonard, L. J., Darlington, A., Forbes, D. L., and Craymer, M. (2014). Relative sea-level projections in Canada and the adjacent mainland United States. *Geol. Surv. Canada Open File* 7737:10.4095. doi: 10.4095/295574

Jones, B. M., Arp, C. D., Jorgenson, M. T., Hinkel, K. M., Schmutz, J. A., and Flint, P. L. (2009). Increase in the rate and uniformity of coastline erosion in Arctic Alaska. *Geophys. Res. Lett.* 36, 1–5. doi: 10.1029/2008GL036205

Jones, B. M., Farquharson, L. M., Baughman, C. A., Buzard, R. M., Arp, C. D., Grosse, G., et al. (2018). A decade of remotely sensed observations highlight

complex processes linked to coastal permafrost bluff erosion in the Arctic A decade of remotely sensed observations highlight complex processes linked to coastal permafrost bluff eros. *Environ. Res. Lett.* 13:115001. doi: 10.1088/1748-9326/aae471

Jong, D., Bröder, L., Tanski, G., Fritz, M., Lantuit, H., Tesi, T., et al. (2020). Nearshore zone dynamics determine pathway of organic carbon from eroding permafrost coasts. *Geophys. Res. Lett.* 47:e2020GL088561. doi: 10.1029/2020GL088561

Karlsson, E. S., Brüchert, V., Tesi, T., Charkin, A., Dudarev, O., Semiletov, I., et al. (2015). Contrasting regimes for organic matter degradation in the East Siberian Sea and the Laptev Sea assessed through microbial incubations and molecular markers. *Mar. Chem.* 170, 11–22. doi: 10.1016/J.MARCHEM.2014.12.005

Kaufman, D. S., Schneider, D. P., McKay, N. P., Ammann, C. M., Bradley, R. S., Briffa, K. R., et al. (2009). Recent warming reverses long-term arctic cooling. *Science* 325, 1236–1239. doi: 10.1126/science.1173983

Kennedy, C. E., Smith, C. A. S., and Cooley, D. A. (2001). Observations of change in the cover of polargrass, Arctagrostis latifolia, and arctic lupine, Lupinus arcticus, in upland tundra on Herschel Island, Yukon Territory. *Can. Field Natural.* 115, 323–328.

Killops, S., and Killops, V. (2004). *Introduction to Organic Geochemistry*. Harlow: Longman Scientific & Technical.

Klein, K. P., Lantuit, H., Heim, B., Fell, F., Doxaran, D., and Irrgang, A. M. (2019). Long-term high-resolution sediment and sea surface temperature spatial patterns in arctic nearshore waters retrieved using 30-year landsat archive imagery. *Remote Sens.* 11:2791. doi: 10.3390/rs11232791

Knoblauch, C., Beer, C., Liebner, S., Grigoriev, M. N., and Pfeiffer, E. M. (2018). Methane production as key to the greenhouse gas budget of thawing permafrost. *Nat. Clim. Change* 8, 1–4. doi: 10.1038/s41558-018-0095-z

Knoblauch, C., Beer, C., Sosnin, A., Wagner, D., and Pfeiffer, E. M. (2013). Predicting long-term carbon mineralization and trace gas production from thawing permafrost of Northeast Siberia. *Glob. Change Biol.* 19, 1160–1172. doi: 10.1111/gcb.12116

Kokelj, S. V., Lacelle, D., Lantz, T. C., Tunnicliffe, J., Malone, L., Clark, I. D., et al. (2013). Thawing of massive ground ice in mega slumps drives increases in stream sediment and solute flux across a range of watershed scales. *J. Geophys. Res. Earth Surf.* 118, 681–692. doi: 10.1002/jgrf.20063

Kokelj, S. V., Smith, C. A. S., and Burn, C. R. (2002). Physical and chemical characteristics of the active layer and permafrost, Herschel Island, western Arctic Coast, Canada. *Permafrost Periglac. Process.* 13, 171–185. doi: 10.1002/ppp.417

Kristensen, E., Ahmed, S. I., and Devol, A. H. (1995). Aerobic and anaerobic decomposition of organic matter in marine sediment: which is fastest? *Limnol. Oceanogr.* 40, 1430–1437. doi: 10.4319/lo.1995.40.8.1430

Kuhry, P., and Vitt, D. H. (1996). Fossil carbon/nitrogen ratios as a measure of peat decomposition. *Ecol. Soc. Am.* 77, 271–275. doi: 10.2307/2265676

Kvenvolden, K. (1970). "Evidence for transformation of normal fatty acids in sediments," in *Advances in Organic Geochemistry*, 1966, eds G. D. Hobson and G. C. Speers (Oxford: Pergamon Press), 335–366.

Lamb, A. L., Wilson, G. P., and Leng, M. J. (2006). A review of coastal palaeoclimate and relative sea-level reconstructions using δ13C and C/N ratios in organic material. *Earth Sci. Rev.* 75, 29–57. doi: 10.1016/j.earscirev.2005.10.003

Lantuit, H., Overduin, P. P., Couture, N., Wetterich, S., Aré, F., Atkinson, D., et al. (2012). The arctic coastal dynamics database: a new classification scheme and statistics on arctic permafrost coastlines. *Estuar. Coasts* 35, 383–400. doi: 10.1007/s12237-010-9362-6

Lantuit, H., and Pollard, W. H. (2005). Temporal stereophotogrammetric analysis of retrogressive thaw slumps on Herschel Island, Yukon Territory. *Nat. Haz. Earth Syst. Sci.* 5, 413–423. doi: 10.5194/nhess-5-413-2005

Lantuit, H., and Pollard, W. H. (2008). Fifty years of coastal erosion and retrogressive thaw slump activity on Herschel Island, southern Beaufort Sea, Yukon Territory, Canada. *Geomorphology* 95, 84–102. doi: 10.1016/j.geomorph.2006.07.040

Lee, H., Schuur, E. A. G., Inglett, K. S., Lavoie, M., and Chanton, J. P. (2012). The rate of permafrost carbon release under aerobic and anaerobic conditions and its potential effects on climate. *Glob. Change Biol.* 18, 515–527. doi: 10.1111/j.1365-2486.2011.02519.x

Li, G., Li, L., Tarozo, R., Longo, W. M., Wang, K. J., Dong, H., et al. (2018). Microbial production of long-chain n-alkanes: implication for interpreting sedimentary leaf wax signals. *Organ. Geochem.* 115, 24–31. doi: 10.1016/j.orggeochem.2017.10.005

Littlefair, C. A., Tank, S. E., and Kokelj, S. V. (2017). Retrogressive thaw slumps temper dissolved organic carbon delivery to streams of the Peel Plateau, NWT, Canada. *Biogeosciences* 14, 5487–5505. doi: 10.5194/bg-14-5487-2017

Macdonald, R. W., Kuzyk, Z. Z. A., and Johanessen, S. C. (2015). The vulnerability of Arctic shelf sediments to climate change. *Environ. Rev.* 23, 461–479. doi: 10.1139/er-2015-0040

Mack, M. C., Schuur, E. A. G., Bret-Harte, M. S., Shaver, G. R., and Chapin, F. S. (2004). Ecosystem carbon storage in arctic tundra reduce by long-term nutrient fertilization. *Nature* 431, 440–443. doi: 10.1038/nature02887

Mann, P. J., Eglinton, T. I., McIntyre, C. P., Zimov, N., Davydova, A., Vonk, J. E., et al. (2015). Utilization of ancient permafrost carbon in headwaters of Arctic fluvial networks. *Nat. Commun.* 6:7856. doi: 10.1038/ncomms8856

Manson, G. K., and Solomon, S. M. (2007). Past and future forcing of Beaufort Sea coastal change. *Atmosphere Ocean* 45, 107–122. doi: 10.3137/ao.450204

Manson, G. K., Solomon, S. M., Forbes, D. L., Atkinson, D. E., and Craymer, M. (2005). Spatial variability of factors influencing coastal change in the Western Canadian Arctic. *Geo Mar. Lett.* 25, 138–145. doi: 10.1007/s00367-004-0195-9

Mathis, J. T., Pickart, R. S., Byrne, R. H., McNeil, C. L., Moore, G. W. K., Juranek, L. W., et al. (2012). Storm-induced upwelling of high p CO_2 waters onto the continental shelf of the western Arctic Ocean and implications for carbonate mineral saturation states. *Geophysical Research Letters* 39, doi: 10.1029/2012GL051574

McGuire, A., Anderson, L., Christensen, T. R., Dallimore, S., Guo, L., Hayes, D., et al. (2009). Sensitivity of the carbon cycle in the Arctic to climate change. *Ecol. Monogr.* 79, 523–555. doi: 10.1890/08-2025.1

McGuire, A. D., Lawrence, D. M., Koven, C., Clein, J. S., Burke, E., and Chen, G. (2018). Dependence of the evolution of carbon dynamics in the northern permafrost region on the trajectory of climate change. *Proc. Natl. Acad. Sci. U.S.A.* 115, 3882–3887. doi: 10.1073/pnas.1719903115

Millero, F., Huang, F., Graham, T., and Pierrot, D. (2007). The dissociation of carbonic acid in NaCl solutions as a function of concentration and temperature. *Geochim. Cosmochim. Acta* 71, 46–55. doi: 10.1016/j.gca.2006.08.041

Naidu, A. S., Cooper, L. W., Finney, B. P., Macdonald, R. W., Alexander, C., and Semiletov, I. P. (2000). Organic carbon isotope ratio ($\delta^{13}C$) of Arctic Amerasian Continental shelf sediments. *Int. J. Earth Sci.* 89, 522–532. doi: 10.1007/s005310000121

Neff, J. C., and Asner, G. P. (2001). Dissolved organic carbon in terrestrial ecosystems: synthesis and a model. *Ecosystems* 4, 29–48. doi: 10.1007/s100210000058

Nielsen, D. M., Dobrynin, M., Baehr, J., Razumov, S., and Grigoriev, M. (2020). Coastal erosion variability at the southern laptev sea linked to winter sea ice and the arctic oscillation. *Geophys. Res. Lett.* 47:e2019GL086876. doi: 10.1029/2019GL086876

Obu, J., Lantuit, H., Fritz, M., Pollard, W. H., Sachs, T., and Günther, F. (2016). Relation between planimetric and volumetric measurements of permafrost coast erosion: a case study from Herschel Island, western Canadian Arctic. *Polar Res.* 35:30313. doi: 10.3402/polar.v35.30313

Obu, J., Lantuit, H., Grosse, G., Günther, F., Sachs, T., Helm, V., et al. (2015). Coastal erosion and mass wasting along the Canadian Beaufort Sea based on annual airborne LiDAR elevation data. *Geomorphology* 293, 331–346. doi: 10.1016/j.geomorph.2016.02.014

Overduin, P. P., Liebner, S., Knoblauch, C., Günther, F., Wetterich, S., Schirrmeister, L., et al. (2015). Methane oxidation following submarine permafrost degradation: measurements from a central Laptev Sea shelf borehole. *J. Geophys. Res. G Biogeosci.* 120, 965–978. doi: 10.1002/2014JG002862

Overeem, I., Anderson, R. S., Wobus, C. W., Clow, G. D., Urban, F. E., and Matell, N. (2011). Sea ice loss enhances wave action at the Arctic coast. *Geophys. Res. Lett.* 38, 1–6. doi: 10.1029/2011GL048681

Pelletier, B. R., and Medioli, B. E. (2014). Environmental atlas of the Beaufort coastlands. *Geol. Surv. Canada Open File* 7619, 1–271. doi: 10.4095/294601

Pipko, I. I., Pugach, S. P., Semiletov, I. P., Anderson, L. G., Shakhova, N. E., Gustafsson, Ö, et al. (2017). The spatial and interannual dynamics of the surface water carbonate system and air-sea CO2 fluxes in the outer shelf and slope of the Eurasian Arctic Ocean. *Ocean Sci.* 13, 997–1016. doi: 10.5194/os-13-997-2017

Pollard, W. (1990). "The nature and origin of ground ice in the Herschel Island area, Yukon Territory," in *Proceedings of the Fifth Canadian Conference on Permafrost*, Pergélisol, 23–30.

Radosavljevic, B., Lantuit, H., Pollard, W. H., Overduin, P., Couture, N., Sachs, T., et al. (2016). Erosion and flooding — threats to coastal infrastructure in the arctic: a case study from Herschel Island, Yukon Territory, Canada. *Estuar. Coasts* 39, 900–915. doi: 10.1007/s12237-015-0046-0

Ramage, J. L., Fortier, D., Hugelius, G., Lantuit, H., and Morgenstern, A. (2019). Distribution of carbon and nitrogen along hillslopes in three valleys on Herschel Island, Yukon Territory, Canada. *Catena* 178, 132–140. doi: 10.1016/j.catena.2019.02.029

Ramage, J. L., Irrgang, A. M., Herzschuh, U., Morgenstern, A., Couture, N., and Lantuit, H. (2017). Terrain controls on the occurrence of coastal retrogressive thaw slumps along the Yukon Coast, Canada. *J. Geophys. Res. Earth Surf.* 122, 1619–1634. doi: 10.1002/2017JF004231

Rampton, V. N. (1982). Quaternary geology of the Yukon Coastal Plain. *Geol. Surv. Canada Bull.* 317:49.

Rasmussen, H., and Jorgensen, B. B. (1992). Microelectrode studies of seasonal oxygen uptake in a coastal sediment: role of molecular diffusion. *Mar. Ecol. Prog. Ser.* 81, 289–303. doi: 10.3354/meps081289

Rielley, G., Collier, R. J., Jones, D. M., and Eglinton, G. (1991). The biogeochemistry of Ellesmere Lake, U.K.-I: source correlation of leaf wax inputs to the sedimentary lipid record. *Organ. Geochem.* 17, 901–912. doi: 10.1016/0146-6380(91)90031-E

Ruff, M., Fahrni, S., Gäggeler, H. W., Hajdas, I., Suter, M., Synal, H. A., et al. (2010). On-line radiocarbon measurements of small samples using elemental analyzer and MICADAS gas ion source. *Radiocarbon* 52, 1645–1656. doi: 10.1017/S003382220005637X

Sánchez-García, L., Vonk, J. E., Charkin, A. N., Kosmach, D., Dudarev, O. V., Semiletov, I. P., et al. (2014). Characterisation of three regimes of collapsing arctic ice complex deposits on the SE Laptev sea coast using biomarkers and dual carbon isotopes. *Permafrost Periglac. Process.* 25, 172–183. doi: 10.1002/ppp.1815

Schädel, C., Bader, M. K. F., Schuur, E. A. G., Biasi, C., Bracho, R., Capek, P., et al. (2016). Potential carbon emissions dominated by carbon dioxide from thawed permafrost soils. *Nat. Clim. Change* 6, 950–953. doi: 10.1038/nclimate3054

Schädel, C., Schuur, E. A. G., Bracho, R., Elberling, B., Knoblauch, C., Lee, H., et al. (2014). Circumpolar assessment of permafrost C quality and its vulnerability over time using long-term incubation data. *Glob. Change Biol.* 20, 641–652. doi: 10.1111/gcb.12417

Schirrmeister, L., Dietze, E., Matthes, H., Grosse, G., Strauss, J., Laboor, S., et al. (2020). The genesis of Yedoma Ice complex permafrost – grain-size endmember modeling analysis from Siberia and Alaska. *Quatern. Sci. J.* 69, 33–53. doi: 10.5194/egqsj-69-33-2020

Schirrmeister, L., Grigoriev, M. N., Strauss, J., Grosse, G., Overduin, P. P., Kholodov, A., et al. (2018). Sediment characteristics of a thermokarst lagoon in the northeastern Siberian Arctic (Ivashkina Lagoon, Bykovsky Peninsula). *Arktos* 4, 1–16. doi: 10.1007/s41063-018-0049-8

Schuur, E. A. G., McGuire, A. D., Grosse, G., Harden, J. W., Hayes, D. J., Hugelius, G., et al. (2015). Climate change and the permafrost carbon feedback. *Nature* 520, 171–179. doi: 10.1038/nature14338

Semiletov, I. P., Pipko, I., Gustafsson, Ö, Anderson, L. G., Sergienko, V., Pugach, S., et al. (2016). Acidification of East Siberian Arctic Shelf waters through addition of freshwater and terrestrial carbon. *Nat. Geosci.* 9, 361–365. doi: 10.1038/NEGO2695

Semiletov, I. P., Shakhova, N. E., Pipko, I. I., Pugach, S. P., Charkin, A. N., Dudarev, O. V., et al. (2013). Space-time dynamics of carbon and environmental parameters related to carbon dioxide emissions in the Buor-Khaya Bay and adjacent part of the Laptev Sea. *Biogeosciences* 10, 5977–5996. doi: 10.5194/bg-10-5977-2013

Shakhova, N., Semiletov, I., Salyuk, A., Yusupov, V., Kosmach, D., and Gustafsson, O. (2010). Extensive methane venting to the atmosphere from sediments of the East Siberian Arctic Shelf. *Science* 327, 1246–1250. doi: 10.1126/science.1182221

Shakhova, N., Semiletov, I., Sergienko, V., Lobkovsky, L., Yusupov, V., Salyuk, A., et al. (2015). The East Siberian Arctic Shelf: towards further assessment of permafrost-related methane fluxes and role of sea ice. *Philos. Trans. R. Soc. A Math. Phys. Eng. Sci.* 373, 20140451. doi: 10.1098/rsta.2014.0451

Smith, C. A. S., Kennedy, C. E., Hargrave, A. E., and McKenna, K. M. (1989). *Soil and Vegetation of Herschel Island, Yukon Soil Survey Report*, Vol. 1. Ottawa, ON: Land Resource Research Centre, Agriculture Canada.

Sollins, P., Spycher, G., and Glassman, C. A. (1984). Net nitrogen mineralization from light- and heavy-fraction forest soil organic matter. *Soil Biol. Biochem.* 16, 31–37. doi: 10.1016/0038-0717(84)90122-6

Solomon, S. M. (2005). Spatial and temporal variability of shoreline change in the Beaufort-Mackenzie region, northwest territories, Canada. *Geo Mar. Lett.* 25, 127–137. doi: 10.1007/s00367-004-0194-x

Spencer, R. G. M., Mann, P. J., Dittmar, T., Eglinton, T. I., McIntyre, C., Holmes, R. M., et al. (2015). Detecting the signature of permafrost thaw in Arctic rivers. *Geophys. Res. Lett. Res. Lett.* 42, 2830–2835. doi: 10.1002/2015GL063498

Stein, R., and Macdonald, R. W. (2004). *The Arctic Organic Carbon Cycle: Present and Past*. Berlin: Springer.

Stevenson, F. J. (1994). *Humus Chemistry: Genesis, Composition, Reactions*. New York, NY: John Wiley & Sons.

Strauss, J., Schirrmeister, L., Mangelsdorf, K., Eichhorn, L., Wetterich, S., and Herzschuh, U. (2015). Organic-matter quality of deep permafrost carbon - A study from Arctic Siberia. *Biogeosciences* 12, 2227–2245. doi: 10.5194/bg-12-2227-2015

Suzuki, Y., Kudoh, S., and Takahashi, M. (1997). Photosynthetic and respiratory characteristics of an Arctic ice algal community living in low light and low temperature conditions. *J. Mar. Syst.* 11, 111–121. doi: 10.1016/S0924-7963(96)00032-2

Tanski, G., Lantuit, H., Ruttor, S., Knoblauch, C., Radosavljevic, B., Strauss, J., et al. (2017). Transformation of terrestrial organic matter along thermokarst-affected permafrost coasts in the Arctic. *Sci. Total Environ.* 581–582, 434–447. doi: 10.1016/j.scitotenv.2016.12.152

Tanski, G., Wagner, D., Knoblauch, C., Fritz, M., Sachs, T., and Lantuit, H. (2019). Rapid CO2 release from eroding permafrost in seawater. *Geophys. Res. Lett.* 46, 11244–11252. doi: 10.1029/2019GL084303

Vonk, J. E., and Gustafsson, O. (2013). Permafrost-carbon complexities. *Nat. Geosci.* 6, 675–676. doi: 10.1038/ngeo1937

Vonk, J. E., Sánchez-García, L., Semiletov, I., Dudarev, O., Eglinton, T., Andersson, A., et al. (2010). Molecular and radiocarbon constraints on sources and degradation of terrestrial organic carbon along the Kolyma paleoriver transect. East Siberian Sea. *Biogeosciences* 7, 3153–3166. doi: 10.5194/bg-7-3153-2010

Vonk, J. E., Sánchez-García, L., van Dongen, B. E., Alling, V., Kosmach, D., Charkin, A., et al. (2012). Activation of old carbon by erosion of coastal and subsea permafrost in Arctic Siberia. *Nature* 489, 137–140. doi: 10.1038/nature11392

Vonk, J. E., Semiletov, I. P., Dudarev, O. V., Eglinton, T. I., Andersson, A., Shakhova, N., et al. (2014). Preferential burial of permafrost-derived organic carbon in Siberian-Arctic shelf waters. *J. Geophys. Res. Oceans* 119, 8410–8421. doi: 10.1002/2014JC010261

Vonk, J. E., Tank, S. E., Mann, P. J., Spencer, R. G. M., Treat, C. C., Striegl, R. G., et al. (2015). Biodegradability of dissolved organic carbon in permafrost soils and waterways: a meta-analysis. *Biogeosci. Discuss.* 12, 8353–8393. doi: 10.5194/bgd-12-8353-2015

Walz, J., Knoblauch, C., Böhme, L., and Pfeiffer, E.-M. (2017). Regulation of soil organic matter decomposition in permafrost-affected Siberian tundra soils - Impact of oxygen availability, freezing and thawing, temperature, and labile organic matter. *Soil Biol. Biochem.* 110, 34–43. doi: 10.1016/j.soilbio.2017.03.001

Ward, C. P., and Cory, R. M. (2016). Complete and partial photo-oxidation of dissolved organic matter draining permafrost soils. *Environ. Sci. Technol.* 50, 3545–3553. doi: 10.1021/acs.est.5b05354

Ward, R. D. (2020). Sedimentary response of Arctic coastal wetlands to sea level rise. *Geomorpholgy* 370:107400. doi: 10.1016/j.geomorph.2020.107400

Wegner, C., Bennett, K. E., de Vernal, A., Forwick, M., Fritz, M., Heikkila, M., et al. (2015). Variability in transport of terrigenous material on the shelves and the deep Arctic Ocean during the Holocene. *Polar Res.* 34, 1–19. doi: 10.3402/polar.v34.24964

Welte, D. H., and Waples, D. W. (1973). Über die Bevorzugung geradzahliger n-Alkane in Sedimentgesteinen. *Naturwissenschaften* 60, 516–517.

Wild, B., Gentsch, N., Capek, P., Diáková, K., Alves, R. J. E., Bárta, J., et al. (2016). Plant-derived compounds stimulate the decomposition of organic matter in arctic permafrost soils. *Sci. Rep.* 6:25607. doi: 10.1038/srep25607

Wild, B., Schnecker, J., Alves, R. J. E., Barsukov, P., Bárta, J., Čapek, P., et al. (2014). Input of easily available organic C and N stimulates microbial decomposition of soil organic matter in arctic permafrost soil. *Soil Biol. Biochem.* 75, 143–151. doi: 10.1016/j.soilbio.2014.04.014

Wolf-Gladrow, D. A., Zeebe, R. E., Klaas, C., Körtzinger, A., and Dickson, A. G. (2007). Total alkalinity: the explicit conservative expression and its application to biogeochemical processes. *Mar. Chem.* 106, 287–300. doi: 10.1016/j.marchem.2007.01.006

Wolter, J., Lantuit, H., Fritz, M., Macias-Fauria, M., Myers-Smith, I., and Herzschuh, U. (2016). Vegetation composition and shrub extent on the Yukon coast, Canada, are strongly linked to ice-wedge polygon degradation. *Polar Res.* 35:27489. doi: 10.3402/polar.v35.27489

Zolkos, S., Tank, S. E., and Kokelj, S. V. (2018). Mineral weathering and the permafrost carbon-climate feedback. *Geophys. Res. Lett.* 45, 9623–9632. doi: 10.1029/2018GL078748

Conflict of Interest: The authors declare that the research was conducted in the absence of any commercial or financial relationships that could be construed as a potential conflict of interest.